TTP15-015

Topological amplitudes in D decays to two pseudoscalars: a global analysis with linear $SU(3)_F$ breaking

Sarah Müller [a,b],* Ulrich Nierste [b],† and Stefan Schacht [b‡]
[a] *Institut für Experimentelle Kernphysik, Karlsruher Institut für Technologie, D-76021 Karlsruhe, Germany*
[b] *Institut für Theoretische Teilchenphysik, Karlsruher Institut für Technologie, D-76128 Karlsruhe, Germany*

We study decays of D^0, D^+, and D_s^+ mesons into two pseudoscalar mesons by expressing the decay amplitudes in terms of topological amplitudes. Including consistently $\mathrm{SU}(3)_F$ breaking to linear order, we show how the topological-amplitude decomposition can be mapped onto the standard expansion using reduced amplitudes characterized by SU(3) representations. The tree and annihilation amplitudes can be calculated in factorization up to corrections which are quadratic in the color-counting parameter $1/N_c$. We find new sum rules connecting $D^+ \to K_S K^+$, $D_s^+ \to K_S \pi^+$ and $D^+ \to K^+ \pi^0$, which test the quality of the $1/N_c$ expansion. Subsequently, we determine the topological amplitudes in a global fit to the data, taking the statistical correlations among the various measurements into account. We carry out likelihood ratio tests in order to quantify the role of specific topological contributions. While the $\mathrm{SU}(3)_F$ limit is excluded with a significance of more than five standard deviations, a good fit (with $\Delta\chi^2 < 1$) can be obtained with less than 28% of $\mathrm{SU}(3)_F$ breaking in the decay amplitudes. The magnitude of the penguin amplitude P_{break}, which probes the Glashow Iliopoulos Maiani (GIM) mechanism, is consistent with zero; the hypothesis $P_{\mathrm{break}} = 0$ is rejected with a significance of just 0.7σ. We obtain the Standard-Model correlation between $\mathcal{B}(D^0 \to K_L \pi^0)$ and $\mathcal{B}(D^0 \to K_S \pi^0)$, which probes doubly Cabibbo-suppressed amplitudes, and find that $\mathcal{B}(D^0 \to K_L \pi^0) < \mathcal{B}(D^0 \to K_S \pi^0)$ holds with a significance of more than 4σ. We finally predict $\mathcal{B}(D_s^+ \to K_L K^+) = 0.012^{+0.007}_{-0.002}$ at 3σ CL.

I. INTRODUCTION

While there is a plethora of experimental information on hadronic charm decays, no theoretical method for dynamical, QCD-based predictions for the corresponding decay amplitudes is known. The best theoretical approach uses the approximate $\mathrm{SU}(3)_F$ symmetry of the QCD Lagrangian to relate the amplitudes of different decay modes to each other. If one assumes this symmetry to be exact, one can express the amplitudes of all measured decay modes in terms of a smaller number of parameters, which are the reduced amplitudes characterized by $\mathrm{SU}(3)_F$ quantum numbers. Then one can predict the less precisely measured branching fraction on the basis of exact $\mathrm{SU}(3)_F$ or assess the validity of this assumption from the overall quality of the fit [1–14]. $\mathrm{SU}(3)_F$ is broken, because the masses $m_{u,d,s}$ of the three lightest quarks are not equal. Comparing the differences among these masses with a typical hadronic scale one estimates $\mathrm{SU}(3)_F$ breaking to be around 30%. In practice the quality of $\mathrm{SU}(3)_F$ symmetry can be much better (e.g. in heavy-hadron spectroscopy) or much worse (e.g. in heavy-quark fragmentation) and should be critically assessed for each system to which it is applied. Linear (i.e. first-order) $\mathrm{SU}(3)_F$ breaking can be rigorously included into the parameterization of the amplitudes, at the expense of a larger number of reduced amplitudes. In the case of $D \to PP'$, where $D = D^0$, D^+ or D_s^+ and P, P' represent pseudoscalar mesons, such studies have been performed in Refs. [15–28]. (Remarkably, one can find relations between amplitudes which even hold to first order in $\mathrm{SU}(3)_F$ breaking [29].) Since there are less $D \to PP'$ branching fractions than real parameters, there is a multi-dimensional space of solutions (all giving a perfect χ^2) for the latter. Many of these solutions involve reduced $\mathrm{SU}(3)_F$-breaking amplitudes whose sizes are indeed of order 30% or less than the $\mathrm{SU}(3)_F$-leading ones, giving evidence (but no proof) that the $\mathrm{SU}(3)_F$ expansion works. The redundancy associated with the multi-dimensional space of solutions poses a challenge for the numerical method to find the best-fit solutions because of the many flat directions in the space of reduced amplitudes.

An alternative way to parameterize decay amplitudes involves topological amplitudes which are characterized by the flavor flow in the decays [5, 8–11, 13–17, 19, 28, 30–32]. The building blocks of this approach are shown in Tab. I and Fig. 1. The topological amplitudes permit an easy and intuitive implementation of $\mathrm{SU}(3)_F$ relations. They further have the merit that they categorize the decays by dynamical criteria (i.e. whether the valence quark takes part in the weak interaction and which meson picks it up) and permit the combination of $\mathrm{SU}(3)_F$ methods with other calculational methods. In this paper we take a first step in this direction and apply the $1/N_c$ expansion (first applied to D decays in Ref. [33]) to the tree (T) and annihilation (A) amplitudes of Tab. I. ($N_c = 3$ is the number of colors.) T and A each factorize into

*Electronic address: sarah.mueller2@kit.edu
†Electronic address: ulrich.nierste@kit.edu
‡Electronic address: stefan.schacht@kit.edu

the product of a form factor and a decay constant up to corrections of order $1/N_c^2$. We further include linear $\mathrm{SU}(3)_F$ breaking in the topological-amplitude decomposition, similarly to the study of B decays in Ref. [19]. For fixed values of T and A (obtained by adding a chosen $1/N_c^2$ deviation to the factorized expressions) the number of fitted complex topological amplitudes is reduced from 17 to nine, so that the problem of flat directions is substantially alleviated.

The purpose of this paper is a systematic determination of the topological amplitudes including linear $\mathrm{SU}(3)_F$ breaking from a global fit to 16 $D \to PP'$ branching fractions and the measured strong-phase difference $\delta_{K^+\pi^-}$. For each topological amplitude we quantify the amount of $\mathrm{SU}(3)_F$ breaking with statistical likelihood-ratio tests using the statistical package *my*Fitter [34]. The latter is especially convenient in order to include nonlinear constraints in a frequentist analysis using the SLSQP algorithm implemented in `SciPy` [35, 36]. As a novel feature our statistical analysis fully includes the statistical correlations between the different experimental inputs. The ranges of the topological amplitudes found by us are an important input for the prediction of CP asymmetries. However, the latter also involve quantities which cannot be extracted from branching fractions ($\mathrm{SU}(3)_F$ triplet amplitudes), so that additional input is needed for this purpose. This is one reason why we do not include measurements of CP asymmetries in our fit input. The other reason is their sensitivity to new physics, whose quantification should be separated from the determination of hadronic parameters as much as possible. In this paper we also do not consider decays into final states with η or η', which involve additional parameters.

The paper is organized as follows: In Sec. II we present the parameterization of D decay amplitudes using topological amplitudes. We discuss the inclusion of linear $\mathrm{SU}(3)_F$ breaking and the appearing parametric redundancies in the diagrammatic language. In Sec. III we combine the method with $1/N_c$ counting and define our measures of $\mathrm{SU}(3)_F$ breaking. In Sec. IV we present the result of our fit. Finally, we conclude.

II. DIAGRAMMATIC PARAMETERIZATION OF CHARM DECAYS

A. Notation

We choose the following conventions for the meson states:

$$\left|K^+\right\rangle = |u\bar{s}\rangle\,, \qquad \left|K^0\right\rangle = |d\bar{s}\rangle\,, \tag{1}$$

$$\left|K^-\right\rangle = -|s\bar{u}\rangle\,, \qquad \left|\bar{K}^0\right\rangle = \left|s\bar{d}\right\rangle\,, \tag{2}$$

$$\left|\pi^+\right\rangle = \left|u\bar{d}\right\rangle\,, \qquad \left|\pi^0\right\rangle = \frac{1}{\sqrt{2}}\left(\left|d\bar{d}\right\rangle - |u\bar{u}\rangle\right)\,, \tag{3}$$

$$\left|\pi^-\right\rangle = -|d\bar{u}\rangle\,, \qquad \left|D^0\right\rangle = -|c\bar{u}\rangle\,, \tag{4}$$

$$\left|D^+\right\rangle = \left|c\bar{d}\right\rangle\,, \qquad \left|D_s^+\right\rangle = |c\bar{s}\rangle\,. \tag{5}$$

Here the "=" sign means that the flavor quantum numbers of the meson state on the left-hand side equal those of the quark-antiquark state on the right-hand side. Tab. I shows the topological (flavor-flow) amplitudes. The cross denotes the W-boson exchange encoded in the $\Delta C = 1$ Hamiltonian. We write the Cabibbo-favored (CF), singly Cabibbo-suppressed (SCS), and doubly Cabibbo suppressed (DCS) decays as

$$\mathcal{A}^{\mathrm{CF}}(d) \equiv V_{cs}^* V_{ud} \mathcal{A}(d) \equiv V_{cs}^* V_{ud} \sum_i c_i^d \mathcal{T}_i\,, \tag{6}$$

$$\mathcal{A}^{\mathrm{SCS}}(d) \equiv \lambda_{sd} \mathcal{A}(d) \equiv \lambda_{sd} \sum_i c_i^d \mathcal{T}_i\,, \tag{7}$$

$$\mathcal{A}^{\mathrm{DCS}}(d) \equiv V_{cd}^* V_{us} \mathcal{A}(d) \equiv V_{cd}^* V_{us} \sum_i c_i^d \mathcal{T}_i\,. \tag{8}$$

Here, we defined

$$\lambda_{sd} := (\lambda_s - \lambda_d)/2 := (V_{cs}^* V_{us} - V_{cd}^* V_{ud})/2\,, \tag{9}$$

where $\lambda_{sd} \simeq \lambda_s \simeq -\lambda_d$. $\mathcal{T}_i$ is a topological amplitude (see Tabs. I, II) and c_i^d is the corresponding coefficient from Tab. III and $d = D \to PP'$ labels the decay mode. There is a CKM-suppressed part $\propto V_{cb}^* V_{ub}$ in SCS amplitudes which can be safely neglected in all branching ratios.

In the limit of unbroken $\mathrm{SU}(3)_F$ symmetry only the tree (T), annihilation (A), color-suppressed (C), and exchange (E) amplitudes are needed to parameterize all $D \to PP'$ decays. While the penguin amplitude $P_{s,d,b}$ (labeled with the quark flavor running in the loop) is also non-vanishing in unbroken $\mathrm{SU}(3)_F$, it only appears in the combination

$$P_{\mathrm{break}} \equiv P_s - P_d, \tag{10}$$

where we have adopted the notation of Ref. [27]. T,A,C, and E are commonly fitted together with the penguin amplitude P_{break}, which vanishes in the $\mathrm{SU}(3)_F$ limit [9–11, 13, 19, 28, 37]. The normalization of the amplitudes is such that

$$\mathcal{B}(D \to P_1 P_2) = |\mathcal{A}^X(D \to P_1 P_2)|^2 \times \mathcal{P}(D, P_1, P_2)\,, \tag{11}$$

$$\mathcal{P}(D, P_1, P_2) \equiv \tau_D \times \frac{1}{16\pi m_D^3} \times \sqrt{(m_D^2 - (m_{P_1} - m_{P_2})^2)(m_D^2 - (m_{P_1} + m_{P_2})^2)}\,. \tag{12}$$

with $X = \mathrm{CF}, \mathrm{SCS}, \mathrm{DCS}$. In the following, we will only make use of the notation $\mathcal{A}(d)$ without superscript, see Eqs. (6–8).

B. SU(3)$_F$-breaking

Any perturbative treatment starts with a subdivision of the Hamiltonian $H = H_0 + H_1$ into a piece H_0 treated

Name	Diagrams
T	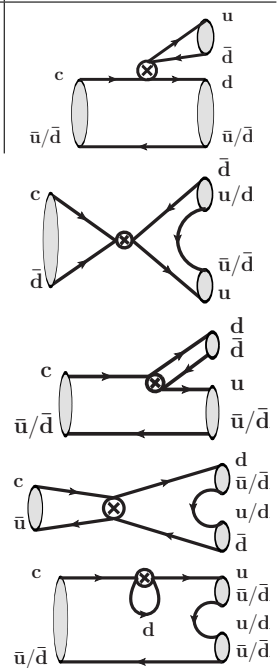

Name	$s-d$ difference of topologies	denoted by Feynman rule
$T_1^{(1)}$	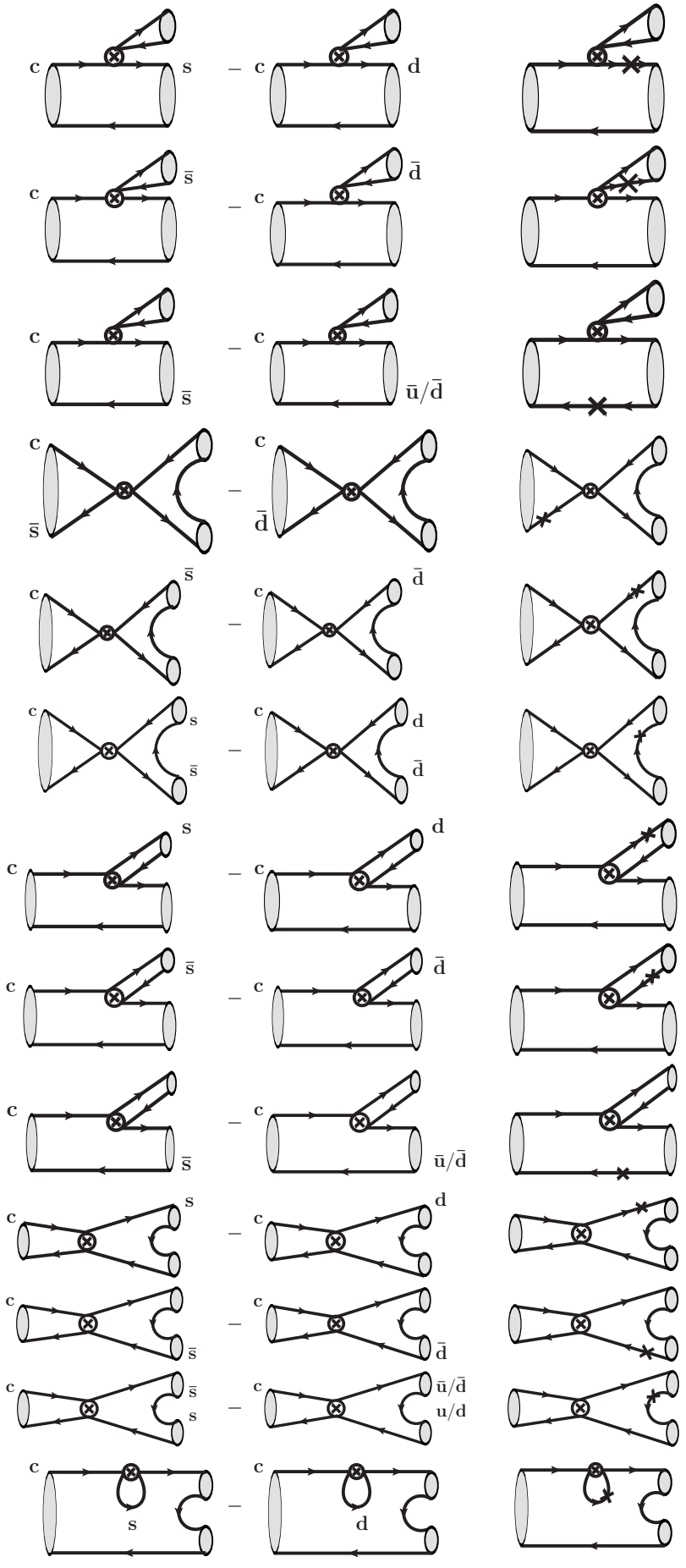	

Decay ampl. $\mathcal{A}(d)$	T	$T_1^{(1)}$	$T_2^{(1)}$	$T_3^{(1)}$	A	$A_1^{(1)}$	$A_2^{(1)}$	$A_3^{(1)}$	C	$C_1^{(1)}$	$C_2^{(1)}$	$C_3^{(1)}$	E	$E_1^{(1)}$	$E_2^{(1)}$	$E_3^{(1)}$	$P_{\rm break}$
SCS																	
$\mathcal{A}(D^0 \to K^+K^-)$	1	1	1	0	0	0	0	0	0	0	0	0	1	1	1	0	1
$\mathcal{A}(D^0 \to \pi^+\pi^-)$	-1	0	0	0	0	0	0	0	0	0	0	0	-1	0	0	0	1
$\mathcal{A}(D^0 \to \bar{K}^0K^0)$	0	0	0	0	0	0	0	0	0	0	0	0	0	-1	-1	1	0
$\mathcal{A}(D^0 \to \pi^0\pi^0)$	0	0	0	0	0	0	0	0	$-\frac{1}{\sqrt{2}}$	0	0	0	$\frac{1}{\sqrt{2}}$	0	0	0	$-\frac{1}{\sqrt{2}}$
$\mathcal{A}(D^+ \to \pi^0\pi^+)$	$-\frac{1}{\sqrt{2}}$	0	0	0	0	0	0	0	$-\frac{1}{\sqrt{2}}$	0	0	0	0	0	0	0	0
$\mathcal{A}(D^+ \to \bar{K}^0K^+)$	1	1	1	0	-1	0	0	-1	0	0	0	0	0	0	0	0	1
$\mathcal{A}(D_s^+ \to K^0\pi^+)$	-1	0	0	-1	1	1	1	0	0	0	0	0	0	0	0	0	1
$\mathcal{A}(D_s^+ \to K^+\pi^0)$	0	0	0	0	$-\frac{1}{\sqrt{2}}$	$-\frac{1}{\sqrt{2}}$	$-\frac{1}{\sqrt{2}}$	0	$-\frac{1}{\sqrt{2}}$	0	0	$-\frac{1}{\sqrt{2}}$	0	0	0	0	$-\frac{1}{\sqrt{2}}$
CF																	
$\mathcal{A}(D^0 \to K^-\pi^+)$	1	1	0	0	0	0	0	0	0	0	0	0	1	1	0	0	0
$\mathcal{A}(D^0 \to \bar{K}^0\pi^0)$	0	0	0	0	0	0	0	0	$\frac{1}{\sqrt{2}}$	$\frac{1}{\sqrt{2}}$	0	0	$-\frac{1}{\sqrt{2}}$	$-\frac{1}{\sqrt{2}}$	0	0	0
$\mathcal{A}(D^+ \to \bar{K}^0\pi^+)$	1	1	0	0	0	0	0	0	1	1	0	0	0	0	0	0	0
$\mathcal{A}(D_s^+ \to \bar{K}^0K^+)$	0	0	0	0	1	1	0	1	1	1	0	1	0	0	0	0	0
DCS																	
$\mathcal{A}(D^0 \to K^+\pi^-)$	1	0	1	0	0	0	0	0	0	0	0	0	1	0	1	0	0
$\mathcal{A}(D^0 \to K^0\pi^0)$	0	0	0	0	0	0	0	0	$\frac{1}{\sqrt{2}}$	0	$\frac{1}{\sqrt{2}}$	0	$-\frac{1}{\sqrt{2}}$	0	$-\frac{1}{\sqrt{2}}$	0	0
$\mathcal{A}(D^+ \to K^0\pi^+)$	0	0	0	0	1	0	1	0	1	0	1	0	0	0	0	0	0
$\mathcal{A}(D^+ \to K^+\pi^0)$	$\frac{1}{\sqrt{2}}$	0	$\frac{1}{\sqrt{2}}$	0	$-\frac{1}{\sqrt{2}}$	0	$-\frac{1}{\sqrt{2}}$	0	0	0	0	0	0	0	0	0	0
$\mathcal{A}(D_s^+ \to K^0K^+)$	1	0	1	1	0	0	0	0	1	0	1	1	0	0	0	0	0

TABLE III: The coefficients of the decomposition of the physical amplitudes (including $\mathrm{SU}(3)_F$ breaking) in terms of the topological amplitudes as in Eqs. (6–8). The table entries are the elements of the coefficient matrix M in Eq. (17).

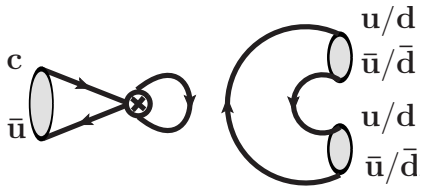

FIG. 1: Penguin annihilation diagram.

Decay d	$PA_{\rm break}$
SCS	
$D^0 \to K^+K^-$	1
$D^0 \to \pi^+\pi^-$	1
$D^0 \to \bar{K}^0K^0$	-1
$D^0 \to \pi^0\pi^0$	$-\frac{1}{\sqrt{2}}$
$D^+ \to \pi^0\pi^+$	0
$D^+ \to \bar{K}^0K^+$	0
$D_s^+ \to K^0\pi^+$	0
$D_s^+ \to K^+\pi^0$	0

TABLE IV: The coefficients of the topological amplitude $PA_{\rm break}$ which is absorbed into E, $E_{1,2,3}^{(1)}$ in Tab. III as explained in Sec. II C.

one can either simply remove redundant parameters and quote numbers for the linear combinations of the topological amplitudes which are in one-to-one correspondence with the physical ones. Or one can use further theoretical (and experimental) input to constrain the topological amplitudes. We determine redundancies among $T, \dots P_{\rm break}$ in this section and relegate the second approach to Sec. III.

The first redundancy is related to $PA_{\rm break}$ of Fig. 1, which appears in SCS decays with the coefficients in Tab. IV. The listed column of coefficients is linearly dependent on the four columns of coefficients of E, $E_{1,2,3}^{(1)}$ in Tab. III. I.e. we can absorb $PA_{\rm break}$ into the exchange amplitudes by redefining $E = \widehat{E} - PA_{\rm break}$, $E_{1,2,3}^{(1)} = \widehat{E}_{1,2,3}^{(1)} + PA_{\rm break}$. In Tab. III this redefinition is implicitly already performed, so that $PA_{\rm break}$ is not shown there anymore. The physical meaning of E, $E_i^{(1)}$ changes accordingly, to be read as $\widehat{E}$, $\widehat{E}_i^{(1)}$ with the penguin annihilation mechanism included. However, $|PA_{\rm break}|$ is expected to be negligibly small: The corresponding Wilson

$\mathbf{p}$	$\mathbf{n}_1$	$\mathbf{n}_2$	$\mathbf{n}_3$	$\mathbf{n}_4$	$\mathbf{n}_5$	$\mathbf{n}_6$	$\mathbf{p}-P_{\rm brk}\mathbf{n}_1$	$\mathbf{p}-A\mathbf{n}_4$	$\mathbf{p}-A_3^{(1)}\mathbf{n}_5$
T	1	1	0	1	0	0	$T-P_{\rm brk}$	$T-A$	T
$T_1^{(1)}$	-1	-1	1	0	0	0	$T_1^{(1)}+P_{\rm brk}$	$T_1^{(1)}$	$T_1^{(1)}$
$T_2^{(1)}$	-1	0	-1	0	0	0	$T_2^{(1)}+P_{\rm brk}$	$T_2^{(1)}$	$T_2^{(1)}$
$T_3^{(1)}$	0	0	0	0	0	-1	$T_3^{(1)}$	$T_3^{(1)}$	$T_3^{(1)}$
A	0	0	0	1	-1	0	A	0	$A+A_3^{(1)}$
$A_1^{(1)}$	0	0	1	0	0	-1	$A_1^{(1)}$	$A_1^{(1)}$	$A_1^{(1)}$
$A_2^{(1)}$	0	1	-1	0	1	0	$A_2^{(1)}$	$A_2^{(1)}$	$A_2^{(1)}-A_3^{(1)}$
$A_3^{(1)}$	0	0	0	0	1	0	$A_3^{(1)}$	$A_3^{(1)}$	0
C	-1	-1	0	-1	0	0	$C+P_{\rm brk}$	$C+A$	C
$C_1^{(1)}$	1	1	-1	0	0	0	$C_1^{(1)}-P_{\rm brk}$	$C_1^{(1)}$	$C_1^{(1)}$
$C_2^{(1)}$	1	0	1	0	0	0	$C_2^{(1)}-P_{\rm brk}$	$C_2^{(1)}$	$C_2^{(1)}$
$C_3^{(1)}$	0	0	0	0	0	1	$C_3^{(1)}$	$C_3^{(1)}$	$C_3^{(1)}$
E	0	-1	0	-1	0	0	E	$E+A$	E
$E_1^{(1)}$	0	1	-1	0	0	0	$E_1^{(1)}$	$E_1^{(1)}$	$E_1^{(1)}$
$E_2^{(1)}$	0	0	1	0	0	0	$E_2^{(1)}$	$E_2^{(1)}$	$E_2^{(1)}$
$E_3^{(1)}$	0	1	0	0	0	0	$E_3^{(1)}$	$E_3^{(1)}$	$E_3^{(1)}$
$P_{\rm brk}$	1	0	0	0	0	0	0	$P_{\rm brk}$	$P_{\rm brk}$

TABLE V: The parameter vector $\mathbf{p}$ as defined in Eq. (16), vectors $\mathbf{n}_i$ spanning the kernel of the coefficient matrix M in Tab. III, and several redefined parameter vectors, see Eqs. (18–20).

coefficient in H_W is small and the momentum flowing through the penguin loop is large (of order of the D^0 mass) so that the Glashow-Iliopoulos-Maiani (GIM) [38] suppression will be effective.

Further redundancies are related to the fact that our coefficient matrix M in Eq. (17) does not have maximal rank. Considering first the $\mathrm{SU}(3)_F$ limit ignoring $T_i^{(1)}, A_i^{(1)}, C_i^{(1)}$, and $E_i^{(1)}$ one observes that the remaining matrix in Tab. III linking T, C, A and E to the physical amplitudes has only rank three. I.e. one of T, C, A and E is redundant.

Redundancies of the diagrammatic approach in the $\mathrm{SU}(3)_F$ limit are also discussed in Ref. [9], comparing to the $\mathrm{SU}(3)_F$ parametrization in Ref. [7]. The corresponding matching for B decays is done in Ref. [10]. Note that the redundancies change when taking $\eta^{(\prime)}$ final states into account [14, 23], leading to more parameters but also additional sum rules [29].

Including $\mathrm{SU}(3)_F$ breaking, the 17×17 matrix M in Tab. III has rank 11. Consequently $\mathbf{p}$ in Eq. (16) contains six redundant complex parameters. The remaining parametric redundancy contained in Tab. III can be systematically found and removed as follows. It is encoded in the six-dimensional kernel of the coefficient matrix. The 17-dimensional basis vectors of the kernel are given in column 2 to 7 of Tab. V. If we redefine $\mathbf{p}$ in Eq. (16) as

$$\mathbf{p}^{\rm new} \equiv \mathbf{p} + \sum_i c_i \mathbf{n}_i\,, \quad c_i \in \mathbb{C}\,, \tag{18}$$

this will not change $M\mathbf{p}$ in Eq. (17), i.e. the $\mathbf{n}_i$ define the "flat directions" in parameter space which correspond to the same $\boldsymbol{\mathcal{A}}$. One can remove this redundancy by redefining the topological amplitudes and choosing 11 of them as new independent parameters. For example we can set

$$\tilde{\mathbf{p}}^{\rm new} \equiv \mathbf{p} - P_{\rm break}\mathbf{n}_1 \tag{19}$$

which gives the result in the first column after the double line in Tab. V. Subsequently, we can redefine the parameters in order to eliminate $P_{\rm break}$. In order to remove all redundancies in one step one can choose

$$\begin{aligned}\hat{\mathbf{p}}^{\rm new} \equiv \mathbf{p} - P_{\rm break}\mathbf{n}_1 - E_3^{(1)}\mathbf{n}_2 - E_2^{(1)}\mathbf{n}_3 - \\ A\mathbf{n}_4 - A_3^{(1)}(\mathbf{n}_4+\mathbf{n}_5) - C_3^{(1)}\mathbf{n}_6\end{aligned} \tag{20}$$

and then perform redefinitions of the other parameters in order to remove

$$P_{\rm break}\,, E_3^{(1)}\,, E_2^{(1)}\,, A\,, A_3^{(1)}\,, C_3^{(1)} \tag{21}$$

from the parameterization. Note the special form of $\mathbf{n}_4$ which encodes the redundancy present in the $\mathrm{SU}(3)_F$ limit. $\mathbf{n}_4$ forces us to eliminate one of T, C, E, or A, while the other five eliminations involve $\mathrm{SU}(3)_F$-breaking amplitudes (e.g. those in Eq. (21)). The elimination of A only is also shown in Tab. V. Additionally, from $\mathbf{n}_5$ we see that the coefficient vector of $A_3^{(1)}$ is linearly dependent on the other annihilation coefficient vectors. Consequently, $A_3^{(1)}$ can be absorbed by redefining annihilation amplitudes only, as shown also explicitly in Tab. V.

Note further that the $\mathbf{n}_i$ are linearly independent also when removing all but the first six elements. This means it is not possible to perform redefinitions without touching the tree or annihilation diagrams. Equivalently, the submatrix obtained by removing tree and annihilation diagrams from Tab. III has rank nine, which in this case equals the number of remaining parameters, i.e. the lower nine components of $\mathbf{p}$. This observation guides us to the approach of Sec. III: calculating tree and annihilation amplitudes will also remove the redundancies.

After absorbing some topological amplitudes (e.g. those in Eq. (21)) into others the new amplitudes have lost their original meaning in terms of QCD dynamics. An important question in charm physics is the level of GIM cancellation between an s and d loop. In this paper we encounter $P_{\rm break}$ as a quantity probing the GIM mechanism. A naive quark-level calculation involves a suppression factor of m_s^2/m_c^2 and renders $P_{\rm break}$ negligibly small. Thus any information on the actual size of $|P_{\rm break}|$ may give insight into a possible non-perturbative enhancement of GIM-suppressed amplitudes. However, as shown above and exemplified in Tab. V the fit to

topological amplitudes alone cannot give this information, because P_{break} cannot be separated from the other parameters fitted from the data.

As we have seen above, the calculation of the kernel gives a method to remove redundant parameters. In the same way, the cokernel of M gives us information on "redundant" amplitudes, i.e. six sum rules fulfilled by the latter, all of which were found in Ref. [29]. In other words: if one did a Gaussian elimination to determine $\mathbf{p}$ from Eq. (17), one would end up with a 6×17 block of zeros in the transformed coefficient matrix M and linear combinations of physical amplitudes in the corresponding six entries of $\boldsymbol{\mathcal{A}}$. These linear combinations vanish by the $\mathrm{SU}(3)_F$ sum rules of Ref. [29]. Thus the discussed redundancies are not the consequence of missing experimental information but of the symmetry relations underlying these sum rules. It is instructive to rederive these sum rules with our diagrammatic method, which is particularly straightforward and intuitive. We do this in Appendix D.

We checked that after the removal of all redundancies, the diagrammatic parameterization and the common expansion in terms of $\mathrm{SU}(3)_F$ representations can be mapped onto each other, i.e. one can calculate one set of parameters when given the other one. The mapping can be obtained explicitly by inverting either the reduced coefficient matrix M or its counterpart in the $\mathrm{SU}(3)_F$ method. Note that in the $\mathrm{SU}(3)_F$ parameterization unphysical degrees of freedom are present in the very same way. Analogously, it is possible to redefine $\mathrm{SU}(3)_F$ matrix elements in order to obtain a physical basis [23]. In Appendix B we give the inverse of the $\mathrm{SU}(3)_F$ coefficient matrix of [23] and show the result of the extraction of the corresponding $\mathrm{SU}(3)_F$ matrix elements for an example fit point of our diagrammatic analysis. So far our discussion of redundancies has assumed that the amplitudes in $\boldsymbol{\mathcal{A}}$ are known. In practice, there is no information on most of their complex phases (and not all of them are physical). This feature introduces additional flat directions in the space of our fit parameters and is equally present in the $\mathrm{SU}(3)_F$ method.

The discussion above has made clear that the topological-amplitude method is complete in the sense that it contains the full information contained in an $\mathrm{SU}(3)_F$ analysis including $\mathrm{SU}(3)_F$ breaking to linear order. It is also worthwhile to study this question from the viewpoint of QCD dynamics: are there any dynamical mechanisms which cannot be mapped onto topological amplitudes? As a first topic we discuss final-state rescattering, i.e. decays $D \to f' \to f$ passing through an on-shell intermediate state f'. The flavor flow for such a rescattering process is always a deformation of a diagram in Tab. I or Fig. 1 and is therefore included in the corresponding topological amplitude. Rescattering effects cannot be isolated from the "direct" $D \to f$ decay, because the dispersive part of $\mathcal{A}(D \to f' \to f)$ cannot be separated from that of $\mathcal{A}(D \to f)$ in a meaningful way. (Neglecting CP violation we can choose phase conventions such that the dispersive and absorptive parts of some amplitude equal its real and imaginary parts, respectively.) By the optical theorem the absorptive part of $\mathcal{A}(D \to f)$ can be related to $\mathcal{A}(D \to f')$ and the $f' \to f$ scattering amplitude, with summation over all intermediate states f'. This feature holds true for the topological amplitudes as well. The imaginary parts of the topological amplitudes found in our fit in Sec. IV are therefore a measure of the size of rescattering. The second topic of QCD dynamics addresses the proper description of meson states. The state of e.g. an energetic kaon can be expanded as

$$\left|K^0\right\rangle = |d\bar{s}\rangle + |d\bar{s}g\rangle + |d\bar{s}q\bar{q}\rangle + \dots\,, \tag{22}$$

where the notation implicitly contains convolution integrals over the kaon momentum fraction carried by the indicated partons. Our graphical description of the topological amplitudes only catches the first term in Eq. (22). The higher Fock states $|d\bar{s}g\rangle\,, |d\bar{s}u\bar{u}\rangle\,, \dots$ are suppressed with powers of the kaon energy, but in view of the small energy release in D decays this suppression is unlikely to be realized numerically. We may wonder whether the contributions with additional $q\bar{q}$ pairs in Eq. (22) will require the introduction of further amplitude topologies, with extra quark lines connected with "sea" quarks in the mesons. An example is shown in Fig. 2. However, it is easy to see that such diagrams are always obtained by forking a quark line of one of the topological amplitudes considered so far. For instance, the diagram in Fig. 2 is contained in P_{break}.

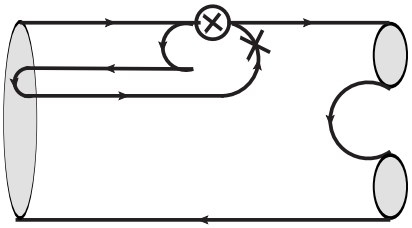

FIG. 2: Example for a $\mathrm{SU}(3)_F$-breaking diagram involving sea quarks which can be absorbed into P_{break}, see Tab. II.

III. THEORETICAL INPUT ON DIAGRAMMATIC $\mathrm{SU}(3)_F$ BREAKING

The great advantage of the flavor-flow parameterization over the plain $\mathrm{SU}(3)_F$ approach is the opportunity to add dynamical input to constrain individual topologies. We use two different such inputs which are presented below.

Decay ampl. $\widetilde{\mathcal{A}}(d)$	$\delta_T-\delta_A$	$\widetilde{C}\equiv C+\delta_A$	$C_1^{(1)}$	$C_2^{(1)}$	$C_3^{(1)}$	$\widetilde{E}\equiv E+\delta_A$	$E_1^{(1)}$	$E_2^{(1)}$	$E_3^{(1)}$	$P_{\rm break}$
SCS										
$\widetilde{\mathcal{A}}(D^0\to K^+K^-)$	1	0	0	0	0	1	1	1	0	1
$\widetilde{\mathcal{A}}(D^0\to \pi^+\pi^-)$	-1	0	0	0	0	-1	0	0	0	1
$\widetilde{\mathcal{A}}(D^0\to \bar K^0K^0)$	0	0	0	0	0	0	-1	-1	1	0
$\widetilde{\mathcal{A}}(D^0\to \pi^0\pi^0)$	0	$-\frac{1}{\sqrt{2}}$	0	0	0	$\frac{1}{\sqrt{2}}$	0	0	0	$-\frac{1}{\sqrt{2}}$
$\widetilde{\mathcal{A}}(D^+\to \pi^0\pi^+)$	$-\frac{1}{\sqrt{2}}$	$-\frac{1}{\sqrt{2}}$	0	0	0	0	0	0	0	0
$\widetilde{\mathcal{A}}(D^+\to \bar K^0K^+)$	1	0	0	0	0	0	0	0	0	1
$\widetilde{\mathcal{A}}(D_s^+\to K^0\pi^+)$	-1	0	0	0	0	0	0	0	0	1
$\widetilde{\mathcal{A}}(D_s^+\to K^+\pi^0)$	0	$-\frac{1}{\sqrt{2}}$	0	0	$-\frac{1}{\sqrt{2}}$	0	0	0	0	$-\frac{1}{\sqrt{2}}$
CF										
$\widetilde{\mathcal{A}}(D^0\to K^-\pi^+)$	1	0	0	0	0	1	1	0	0	0
$\widetilde{\mathcal{A}}(D^0\to \bar K^0\pi^0)$	0	$\frac{1}{\sqrt{2}}$	$\frac{1}{\sqrt{2}}$	0	0	$-\frac{1}{\sqrt{2}}$	$-\frac{1}{\sqrt{2}}$	0	0	0
$\widetilde{\mathcal{A}}(D^+\to \bar K^0\pi^+)$	1	1	1	0	0	0	0	0	0	0
$\widetilde{\mathcal{A}}(D_s^+\to \bar K^0K^+)$	0	1	1	0	1	0	0	0	0	0
DCS										
$\widetilde{\mathcal{A}}(D^0\to K^+\pi^-)$	1	0	0	0	0	1	0	1	0	0
$\widetilde{\mathcal{A}}(D^0\to K^0\pi^0)$	0	$\frac{1}{\sqrt{2}}$	0	$\frac{1}{\sqrt{2}}$	0	$-\frac{1}{\sqrt{2}}$	0	$-\frac{1}{\sqrt{2}}$	0	0
$\widetilde{\mathcal{A}}(D^+\to K^0\pi^+)$	0	1	0	1	0	0	0	0	0	0
$\widetilde{\mathcal{A}}(D^+\to K^+\pi^0)$	$\frac{1}{\sqrt{2}}$	0	0	0	0	0	0	0	0	0
$\widetilde{\mathcal{A}}(D_s^+\to K^0K^+)$	1	1	0	1	1	0	0	0	0	0

TABLE VI: Coefficients of the parameters $(\delta_T-\delta_A,\dots P_{\rm break})$ for the amplitudes $\widetilde{\mathcal{A}}(d)$, which are obtained from $\mathcal{A}(d)$ by subtracting the factorized part, see Eq. (27). The table entries are the elements of the coefficient matrix $\widetilde{M}$ in Eq. (34).

A. $1/N_c$ counting

The $1/N_c$ expansion [39] has first been applied to charm physics in Ref. [33]. We will apply $1/N_c$ counting to the tree and annihilation topologies, which are leading in $1/N_c$. Here we exemplify the method for T:

$$T = T^{\rm fac}+\delta_T, \tag{23}$$

$$T^{\rm fac} \equiv \frac{G_F}{\sqrt{2}} a_1 f_\pi (m_D^2-m_\pi^2) F_0^{D\pi}(m_\pi^2)\,. \tag{24}$$

Here $a_1=C_2+C_1/N_c=1.06$ in terms of the usual Wilson coefficients $C_{1,2}$ of H_W and the quoted value corresponds to next-to-leading order in the NDR scheme at a scale of 1.5 GeV. It is important to note that the color exchange between the two quark lines in the T diagram in Tab. I is penalized by *two* powers of $1/N_c$. We parameterize this $1/N_c^2$ correction by the complex parameter δ_T in Eq. (23). Also the renormalization scale and scheme dependences of a_1 are suppressed by $1/N_c^2$. By using Eq. (23) and the equivalent formulae for the other tree amplitudes $T+T_1^{(1)},\dots$ we trade four parameters for a single parameter δ_T with $|\delta_T/T^{\rm fac}|\le 0.15$. SU(3)$_F$ breaking in this small parameter is neglected, because it is smaller than the neglected second-order SU(3)$_F$-breaking effects. $F_0^{D\pi}(m_\pi^2)$ entering $T^{\rm fac}$ is measured in semileptonic D decays, therefore the $1/N_c$ method uses additional experimental input, too. Also the A amplitudes factorize up to corrections of order $1/N_c^2$. The factorization formulae for all tree and annihilation amplitudes can be found in Appendices C 1 and C 2, respectively. In analogy to δ_T we define the complex parameter

$$\delta_A = A - A^{\rm fac} \tag{25}$$

for the $\mathcal{O}(1/N_c^2)$ corrections. $A^{\rm fac}$ depends on the form factor $F_0^{K\pi}(m^2_{D_{(s)}})$, see Appendix C 2 for details.

E, C, and $P_{\rm break}$ are formally suppressed by one power of $1/N_c$ with respect to T. However, E and C are enhanced by short-distance QCD effects residing in the Wilson coefficients: we write $H_W\propto C_1Q_1+C_2Q_2=(C_1+C_2/N_c)Q_1+2C_2Q_8$ with the octet×octet operator $Q_8\equiv \overline{u}\gamma_\mu T^a c\overline{q}'\gamma^\mu T^a q$ and note that $\langle PP'|\,Q_8\,|D\rangle$ is $1/N_c$ suppressed. However, the Wilson coefficient $2C_2=2.4$ almost exactly offsets the $1/N_c$ suppression, so that E and C can be almost as large as T. We therefore do not place a numerical constraint on $|E|$, $|C|$, or $|P_{\rm break}|$ in our fit but rather keep them general.

With the added $1/N_c$ input the diagrammatic analysis becomes more constrained compared to the plain SU(3)$_F$ approach. Factorization fixes the sizes of the

tree and annihilation amplitudes within roughly $\sim 15\%$ of $T^{\rm fac}$, i.e. the size of the $1/N_c^2$ corrections. In the case of A the $1/N_c^2$ corrections quantified by δ_A include final-state rescattering effects [24, 40–44], which are not proportional to the decay constant f_D which enters $A^{\rm fac}$. We therefore do not normalize δ_A to $A^{\rm fac}$, but instead allow $|\delta_A|$ to be as large as $|\delta_T|$. Factorization has also been used in Refs. [28, 45], but only to estimate $\mathrm{SU}(3)_F$ breaking. We instead use it to constrain the overall sizes of T and A. Note that we treat $T^{\rm fac}$ and $A^{\rm fac}$ beyond linear $\mathrm{SU}(3)_F$ breaking, so that these factorized amplitudes violate the Grossman-Robinson $\mathrm{SU}(3)_F$ sum rules [29].

The parameters δ_T and δ_A replace the first eight entries of $\mathbf{p}$ in Eq. (16) as fit parameters. We use

$$\mathbf{p}' \equiv \Big(\delta_T, \delta_A, C, C_1^{(1)}, C_2^{(1)}, C_3^{(1)}, E, E_1^{(1)}, E_2^{(1)}, E_3^{(1)}, P_{\rm break}\Big)^T , \tag{26}$$

comprising 11 parameters in total. We next derive the equivalent of Eq. (17) for this new set of parameters. To this end we define

$$\widetilde{\mathcal{A}}(d) \equiv \mathcal{A}(d) - \mathcal{A}^{\rm fac}(d) , \tag{27}$$

$$\mathcal{A}^{\rm fac}(d) \equiv T^{\rm fac}(d) + A^{\rm fac}(d) . \tag{28}$$

The 17×11 coefficient matrix linking $\mathbf{p}'$ to $\widetilde{\boldsymbol{\mathcal{A}}} = \Big(\widetilde{\mathcal{A}}(D^0 \to K^+K^-), \ldots \widetilde{\mathcal{A}}(D_s^+ \to K^0K^+)\Big)^T$ has only rank 10. This has two implications: Firstly, there is still a redundant parameter. Secondly, there is a new sum rule among the physical amplitudes. Addressing the first point, the kernel has the 11-dimensional basis vector

$$\mathbf{n} = (-1, -1, 1, 0, 0, 0, 1, 0, 0, 0, 0)^T , \tag{29}$$

where the order of the entries is the same as in Eq. (26). The redefinition

$$\mathbf{p}'' \equiv \mathbf{p}' + \delta_A \, \mathbf{n} \tag{30}$$

with $\mathbf{n}$ as in Eq. (29) absorbs δ_A into C, E and δ_T: setting

$$\widetilde{C} = C + \delta_A , \tag{31}$$

$$\widetilde{E} = E + \delta_A , \tag{32}$$

one observes that the physical amplitudes only depend on $\widetilde{C}$, $\widetilde{E}$, and $\delta_T - \delta_A$. Writing

$$\widetilde{\mathbf{p}} \equiv \Big(\delta_T - \delta_A, \widetilde{C}, C_1^{(1)}, C_2^{(1)}, C_3^{(1)}, \widetilde{E}, E_1^{(1)}, E_2^{(1)}, E_3^{(1)}, P_{\rm break}\Big)^T , \tag{33}$$

the desired equivalent of Eq. (17) reads

$$\widetilde{M}\widetilde{\mathbf{p}} = \widetilde{\boldsymbol{\mathcal{A}}}. \tag{34}$$

with the amplitudes of Eq. (27) on the RHS. The resulting 17×10 coefficient matrix $\widetilde{M}$ with rank 10 is shown in Tab. VI. Addressing the second point, we find the new sum rule

$$\widetilde{\mathcal{A}}(D^+ \to \bar{K}^0K^+) - \widetilde{\mathcal{A}}(D_s^+ \to K^0\pi^+) - 2\sqrt{2}\widetilde{\mathcal{A}}(D^+ \to K^+\pi^0) = 0 , \tag{35}$$

from the cokernel of $\widetilde{M}$. It tests the $1/N_c$ counting and is violated by terms which are linear in $\mathrm{SU}(3)_F$ breaking, but suppressed by two powers of $1/N_c$.

The $1/N_c^2$ corrections parametrised by $\delta_{T,A}$ are varied in smaller ranges than the other fit parameters. If we consider them fixed, there remain nine unknown complex parameters in Eq. (26) and a corresponding coefficient matrix with rank nine, implying a new sum rule. We combine the new rule with the one in Eq. (35) as:

$$\widetilde{\mathcal{A}}(D^+ \to \bar{K}^0K^+) - \widetilde{\mathcal{A}}(D_s^+ \to K^0\pi^+) = 2\,(\delta_T - \delta_A) , \tag{36}$$

$$\widetilde{\mathcal{A}}(D^+ \to K^+\pi^0) = \frac{1}{\sqrt{2}}\,(\delta_T - \delta_A) . \tag{37}$$

The amplitudes in Eq. (35) are related to those with $K_{S,L}$ in the final state as

$$\mathcal{A}(D^+ \to K_{S,L}K^+) = \mp\frac{1}{\sqrt{2}}\mathcal{A}(D^+ \to \bar{K}^0K^+) , \tag{38}$$

$$\mathcal{A}(D_s^+ \to K_{S,L}\pi^+) = \frac{1}{\sqrt{2}}\mathcal{A}(D_s^+ \to K^0\pi^+) , \tag{39}$$

The corresponding branching ratios read:

$$\mathcal{B}(D^+ \to K_{S,L}K^+) = |\lambda_{sd}|^2\,\mathcal{P}(D^+, K^0, K^+) \times \Big|\mathcal{A}^{\rm fac}(D^+ \to \bar{K}^0K^+) + (\delta_T - \delta_A) + P_{\rm break}\Big|^2 , \tag{40}$$

$$\mathcal{B}(D_s^+ \to K_{S,L}\pi^+) = |\lambda_{sd}|^2\,\mathcal{P}(D_s^+, K^0, \pi^+) \times \Big|\mathcal{A}^{\rm fac}(D_s^+ \to K^0\pi^+) - (\delta_T - \delta_A) + P_{\rm break}\Big|^2 , \tag{41}$$

$$\mathcal{B}(D^+ \to K^+\pi^0) = |V_{cd}^*V_{us}|^2\,\mathcal{P}(D^+, K^+, \pi^0) \times \Big|\mathcal{A}^{\rm fac}(D^+ \to K^+\pi^0) + (\delta_T - \delta_A)\Big|^2 , \tag{42}$$

with $\mathcal{P}(D, P_1, P_2)$ as defined in Eq. (12). Eqs. (40–42) permit to probe our combined $\mathrm{SU}(3)_F$ and $1/N_c$ expansion quantitatively, since a too large value of $|\delta_T - \delta_A|$ extracted from Eqs. (40–42) would falsify the method. Furthermore, the size of $|P_{\rm break}|$ gives insight into an important issue of QCD dynamics, the size of the GIM suppression in the difference between strange and down loops.

In Tab. VII we show example fits to the branching ratios Eqs. (40)–(42) only, testing the dependence of the fit result on the $1/N_c^2$ corrections and the broken penguin.

In the first place, we illustrate that the data can easily be accommodated for realistic values of δ_T, δ_A and $P_{\rm break}$ (point 0). Taking these parameters out of the fit (point 1)

Example fit point with minimal χ^2:	Point 0	Point 1	Point 2	Point 3	Exp. Data
Applied Conditions:	None	$P_{\text{break}} = \delta_T = \delta_A = 0$	$\delta_T = \delta_A = 0$	$P_{\text{break}} = 0$	—
$\lvert P_{\text{break}}/T^{\text{fac}}\rvert$	0.25	0	0.54	0	—
$\arg(P_{\text{break}})$	4.33	0	2.21	0	—
$\lvert\delta_T\rvert/T^{\text{fac}}$	0.11	0	0	0.15	—
$\arg(\delta_T)$	3.07	0	0	3.55	—
$\lvert\delta_A\rvert/A^{\text{fac}}$	0.09	0	0	0.11	—
$\arg(\delta_A)$	0.67	0	0	6.28	—
$F_0^{D_sK}(0)/F_0^{D\pi}(0)$	0.96	1.01	0.95	0.97	—
$F_0^{DK}(0)$	0.74	0.72	0.74	0.74	—
$F_0^{D\pi}(0)$	0.64	0.64	0.64	0.64	—
$\lvert F_0^{K\pi}(m^2_{D_{(s)}})\rvert$	2.39	1.99	4.50	1.62	—
$\arg(F_0^{K\pi}(m^2_{D_{(s)}}))$	1.71	4.99	5.13	3.92	—
$T^{\text{fac}}/10^{-6}$ GeV	2.52	2.52	2.52	2.52	—
$T^{\text{fac}}(D^+ \to \bar{K}^0K^+)/10^{-6}$ GeV	3.40	3.34	3.40	3.40	—
$T^{\text{fac}}(D_s^+ \to K^0\pi^+)/10^{-6}$ GeV	-2.53	-2.68	-2.51	-2.57	—
$T^{\text{fac}}(D^+ \to K^+\pi^0)/10^{-6}$ GeV	2.22	2.22	2.22	2.22	—
$A^{\text{fac}}(D_s^+ \to K^0\pi^+)/10^{-6}$ GeV	$-0.18 + i\,1.22$	$0.28 - i\,0.99$	$0.94 - i\,2.12$	$-0.59 - i\,0.59$	—
$A^{\text{fac}}(D^+ \to K^+\pi^0)/10^{-6}$ GeV	$0.10 - i\,0.68$	$-0.16 + i\,0.55$	$-0.53 + i\,1.19$	$0.33 + i\,0.33$	—
$\mathcal{B}(D^+ \to K_SK^+)/10^{-3}$	2.83	4.04	2.85	2.83	2.83 ± 0.16 [46]
$\mathcal{B}(D_s^+ \to K_S\pi^+)/10^{-3}$	1.22	1.22	1.23	1.22	1.22 ± 0.06 †[46–48]
$\mathcal{B}(D^+ \to K^+\pi^0)/10^{-4}$	1.83	1.83	1.72	1.83	1.83 ± 0.26 [46]
χ^2	0.00	63.93	0.20	0.00	—
ν	—	5	3	2	—
Significance of rejection	—	7.0σ	0.03σ	0.0σ	—

TABLE VII: Fits to the branching ratios $\mathcal{B}(D^+ \to K_SK^+)$, $\mathcal{B}(D_s^+ \to K_S\pi^+)$, $\mathcal{B}(D^+ \to K^+\pi^0)$ only, without taking correlations and additional constraints on $\text{SU}(3)_F$ breaking, see Sec. III B, into account. The form factors are varied as described in Sec. IV and Appendices C 1 and C 2. The χ^2 is the one taking into account the three given branching ratios and form factors only. ν are the number of degrees of freedom compared to the fit scenario of point 0. The significance of rejection takes point 0 as null hypothesis. †Our average.

results in a bad description of the data which is rejected at 7σ. It is possible to describe the data with an enhanced broken penguin only (point 2) but also with $P_{\text{break}} = 0$ and adjusting δ_T and δ_A (point 3). A better knowledge of the form factor $F_0^{K\pi}(m^2_{D_{(s)}})$, see Appendix C 2, is crucial in order to disentangle an enhanced penguin from $1/N_c^2$ corrections. This could be provided by future high statistics measurements of τ decays [49, 50].

B. Measuring diagrammatic $\text{SU}(3)_F$ breaking

In order to describe $\text{SU}(3)_F$ breaking in the framework of the diagrammatic approach, we introduce the following measures in analogy to Ref. [23]. We define

$$\delta_X'^{,\mathcal{T}} \equiv \max_d \left| \frac{\mathcal{A}_X^{\mathcal{T}}(d)}{\mathcal{A}(d)} \right| , \tag{43}$$

where $\mathcal{T} = C, E, P_{\text{break}}$ and $\mathcal{A}_X^{\mathcal{T}}(d)$ is the part of the amplitude of decay d stemming from the corresponding $\text{SU}(3)_F$-breaking parameter(s) only. $\mathcal{A}(d)$ denotes the full amplitude of decay d. The parameters defined in Eq. (43) give a measure for the maximal $\text{SU}(3)_F$-breaking contribution to the full amplitude from each topology.

A measure of the maximal $\text{SU}(3)_F$ breaking residing in any of the topologies C, E and P_{break} is therefore

$$\delta_X'^{,\text{topo}} \equiv \max_d \left| \frac{\sum_{\mathcal{T}} \mathcal{A}_X^{\mathcal{T}}(d)}{\mathcal{A}(d)} \right| . \tag{44}$$

Note that the $\text{SU}(3)_F$ breaking stemming from our calculation of the T and A topologies using factorization is not included in the definition Eq. (44).

Furthermore, we quantify the relative $\text{SU}(3)_F$ breaking

of C and E topologies by the measures

$$\delta_X^{C_i^{(1)}/\widetilde{C}} \equiv \left|\frac{C_i^{(1)}}{\widetilde{C}}\right|, \qquad \delta_X^{E_i^{(1)}/\widetilde{E}} \equiv \left|\frac{E_i^{(1)}}{\widetilde{E}}\right|, \tag{45}$$

respectively. In the fit we always demand all the above measures to be $\leq 50\%$. In $\delta_X^{\prime,E}$ and $\delta_X^{\prime,\text{topo}}$ we ignore $\mathcal{B}(D^0 \to \bar{K}^0 K^0)$ when taking the maximum, because this branching ratio vanishes in the $\mathrm{SU}(3)_F$ limit. Note that $E_3^{(1)}$ appears in the omitted channel $D^0 \to \bar{K}^0 K^0$ only, therefore $\delta_X^{\prime,E} = 0$ is insensitive to the size of $E_3^{(1)} \neq 0$. Furthermore, in case an amplitude vanishes at some point in parameter space we also exclude it from the calculation of the maxima in Eqs. (43) and (44).

IV. FIT TO BRANCHING RATIO MEASUREMENTS

In our global fit we use the available measured branching fractions and the strong phase difference $\delta_{K^+\pi^-}$ and impose the theoretical constraints quoted in Sec. III. 18 fit parameters are related to topological amplitudes:

$$\begin{gathered}|\widetilde{C}/T^{\text{fac}}|, \quad \arg(\widetilde{C}), \quad |\widetilde{E}/T^{\text{fac}}|, \quad \arg(\widetilde{E}),\\ |C_i^{(1)}|, \quad \arg(C_i^{(1)}), \quad |E_i^{(1)}|, \quad \arg(E_i^{(1)}),\\ |P_{\text{break}}/T^{\text{fac}}|, \quad \arg(P_{\text{break}}),\end{gathered}$$

with $i = 1, 2, 3$ and T^{fac} is calculated from Eq. (24). We normalize to T^{fac} rather than $T = T^{\text{fac}} + \delta_T$, because our fit is only sensitive to the combination $\delta_T - \delta_A$ and therefore leaves δ_T undetermined. These 18 quantities are supplied by four parameters measuring the $1/N_c^2$ corrections to the tree and annihilation diagrams:

$$|\delta_T|/T^{\text{fac}}, \quad \arg(\delta_T), \quad |\delta_A|/T^{\text{fac}}, \quad \arg(\delta_A)\,.$$

In addition we need five parameters related to form factors:

$$\begin{gathered}F_0^{D_s K}(0)/F_0^{D\pi}(0), \quad F_0^{DK}(0), \quad F_0^{D\pi}(0),\\ |F_0^{K\pi}(m_D^2)|, \quad \arg(F_0^{K\pi}(m_D^2))\,,\end{gathered}$$

and set $F_0^{K\pi}(m_{D_s}^2) = F_0^{K\pi}(m_D^2)$. Altogether these are 27 real parameters, which are fitted to 16 measured branching ratios and one strong phase. The experimental input values, including the respective correlations, are listed in Appendix A. The number of parameters is larger than the number of observables. However, the 27 parameters are subject to 10 constraints on the maximal size of linear $\mathrm{SU}(3)_F$ breaking, see Sec. III B, and the bounds $|\delta_{T,A}| \leq 0.15\, T^{\text{fac}}$. At the global minimum we obtain $\chi^2 = 0.0$, i.e., the parameterization and theoretical input is in perfect agreement with the data. Thus the data are both compatible with our chosen bound on $\mathrm{SU}(3)_F$ breaking (i.e. all measures defined in Sec. III B are smaller than 50%) and the six Grossman-Robinson $\mathrm{SU}(3)_F$ sum rules [29].

In order to study the relative importance of the topological amplitudes for the description of the data, we perform likelihood ratio tests. We look at several scenarios where some of the parameters of our fit are fixed. In order to keep the fit simple, we assume the validity of Wilks' theorem [51], i.e., we calculate the p-value according to [34, 46]

$$p = 1 - P_{\nu/2}\left(\Delta\chi^2/2\right), \tag{46}$$

with the normalized lower incomplete Gamma function $P_{\nu/2}$ depending on the number ν of relatively fixed parameters compared to the full fit. For a general discussion of the assumptions underlying Eq. (46) see Ref. [34].

The results of our likelihood ratio tests are shown in Tab. VIII. This table shows at which significance we can reject a certain hypothesis. For example, we can reject $P_{\text{break}} = 0$ at only $\sim 0.7\sigma$, implying that $P_{\text{break}} = 0$ is well consistent with the data. However, the fit shows a clear need for $\mathrm{SU}(3)_F$ breaking: the $\mathrm{SU}(3)_F$-limit fit with $P_{\text{break}} = E_i^{(1)} = C_i^{(1)} = 0\,\forall\, i$ is rejected at $> 5\sigma$. Looking at the $\mathrm{SU}(3)_F$ breaking in specific topological amplitudes we find a slight tendency towards a stronger $\mathrm{SU}(3)_F$ breaking in the color-suppressed tree than in the exchange diagrams.

In Figs. 3–7 we show plots of the fit parameters, measures of $\mathrm{SU}(3)_F$ breaking and fit predictions for observables. We see that in the multi-parameter space the best-fit solutions cover broad regions and typically several disconnected best-fit regions exist. Considering that there are more parameters than fitted quantities the large degeneracy of the best-fit region is not surprising. It is moot to quote best-fit values for the parameters, because one can move in a wide valley with $\Delta\chi^2 = 0$. We suspect that the alternative approach of a Bayesian analysis would single out a small portion of this $\Delta\chi^2 = 0$ valley as a consequence of the Bayesian prior placed on the fit parameters and the central limit theorem of statistics. Therefore Frequentist analyses like ours are more adequate to the problem.

The phase of $\widetilde{C}$ significantly deviates from 0 and π (see Fig. 3(b)), which points to large rescattering effects. The fit results for $|\widetilde{C}/T^{\text{fac}}|$ and $|\widetilde{E}/T^{\text{fac}}|$, see Fig. 3, show disconnected regions at 95% CL. $\widetilde{C}$ and $\widetilde{E}$ are suppressed by $1/N_c$ but involve a large Wilson coefficient ~ 2.4 as discussed in Sec. III A. Thus only solutions with $|\widetilde{C}/T^{\text{fac}}|, |\widetilde{E}/T^{\text{fac}}| \lesssim 1$ are consistent with $1/N_c$ counting, which singles out one of the three regions in the $|\widetilde{C}/T^{\text{fac}}|$–$|\widetilde{E}/T^{\text{fac}}|$ plane.

The needed maximum size of total $\mathrm{SU}(3)_F$ breaking on the amplitude is given by $\delta_X^{\prime,\text{topo}} \sim 30\%$ in agreement with Ref. [23], as can be read off Fig. 4(d). Note that $\delta_X^{\prime,\text{topo}}$ as well as $\delta_X^{\prime,\mathcal{T}}$ do not measure the average but the maximal size of $\mathrm{SU}(3)_F$ breaking in one of the 17 decay channels except for $D^0 \to \bar{K}^0 K^0$, see Sec. III B. Thus, these measures are very conservative and could in principle be biased by a single channel. However, the need for

Hypothesis	Significance of rejection	$\Delta\chi^2$	dof
$P_{\rm break}=0$	0.7σ	1.3	2
$P_{\rm break}=E_i^{(1)}=C_i^{(1)}=0\,\forall\, i$	$>5\sigma$	431.4	14
$E_i^{(1)}=0\,\forall\, i$	3.0σ	20.3	6
$E=E_i^{(1)}=0\,\forall\, i$	$>5\sigma$	156.4	8
$C_i^{(1)}=0\,\forall\, i$	4.5σ	34.1	6
$C=C_i^{(1)}=0\,\forall\, i$	$>5\sigma$	266931.2	8

TABLE VIII: Results of several likelihood ratio tests. Shown are the obtained χ^2, the relative degrees of freedom (*dof*) of the hypothesis compared to the null hypothesis, which is the full fit, and the significance at which the hypothesis can be rejected.

SU(3)$_F$ breaking in individual parameters can be considerably smaller than 30%, *e.g.*, $|E_i^{(1)}|\sim 0$, $|C_{2,3}^{(1)}|\sim 0$ is well allowed at 1σ, see Figs. 5(a) and 5(c), respectively. Also a $|P_{\rm break}/T|$ below 5% already gives very good fits, see Fig. 6(a). In Fig. 4(c) we see that the same is consistently the case for $\delta_X'^{,P_{\rm break}}$.

From Figs. 4(a) and 4(b) we again see the slight tendency for larger SU(3)$_F$ breaking in the color-suppressed tree topologies compared to the exchange diagrams.

As illustrated in Tab. VII discussed in Sec. III A around Eqs. (40–42), the broken penguin $P_{\rm break}$ is correlated with the parameter $\delta_T-\delta_A$ quantifying $1/N_c^2$ corrections to factorizable amplitudes. This feature can be verified in Fig. 6(c) which shows this correlation. A vanishing penguin $P_{\rm break}\sim 0$ is allowed at the price of $1/N_c$ breaking corrections of order $\gtrsim 15\%$. Note again that this correlation heavily depends on the poorly measured form factor $F_0^{K\pi}(m^2_{D_{(s)}})$. Interestingly, the fit result for $F_0^{K\pi}(m^2_{D_{(s)}})$, see Fig. 7, is not completely flat, showing its nontrivial influence on the branching ratios of charm decays. The branching ratio $\mathcal{B}(D^+\to K^+\pi^0)$ depends on no topological parameters besides δ_T and δ_A. Its fit result, which is given in Fig. 8(a), shows that our assumptions on the ranges for δ_T and δ_A are loose enough to accommodate the measured branching fraction. However, large fit results for $\mathcal{B}(D^+\to K^+\pi^0)$ are slightly disfavored.

We may next ask whether we can use our fit output to predict individual branching fractions better than they are currently measured. Our general finding is as in Fig. 8(a), the fit output for the $\Delta\chi^2$ profiles essentially tracks the fit input. To find non-trivial predictions for future measurements we must study correlations between at least two observables. A nice result is shown in Fig. 8(b) revealing the correlation of $\mathcal{B}(D^0\to K_L\pi^0)$ and $\mathcal{B}(D^0\to K_S\pi^0)$. In the SU(3)$_F$ limit the branching ratios are strongly correlated through their parametric dependence[1]

$$\mathcal{B}(D^0\to K_S\pi^0)\sim |E-C|^2+2\lambda^2|E-C|^2\,, \qquad (47)$$

$$\mathcal{B}(D^0\to K_L\pi^0)\sim |E-C|^2-2\lambda^2|E-C|^2\,, \qquad (48)$$

which implies $\mathcal{B}(D^0\to K_L\pi^0)\lesssim\mathcal{B}(D^0\to K_S\pi^0)$. This relation is a priori absent once SU(3)$_F$-breaking effects are included, because the latter can be larger than $|E-C|$. However, the global fit rejects this possibility: in Fig. 8(b) the region corresponding to 95% CL entirely satisfies $\mathcal{B}(D^0\to K_L\pi^0)<\mathcal{B}(D^0\to K_S\pi^0)$. Performing a dedicated likelihood ratio test we find that $\mathcal{B}(D^0\to K_L\pi^0)<\mathcal{B}(D^0\to K_S\pi^0)$ holds with a significance of more than 4σ. Our fit excludes a large region of the $\mathcal{B}(D^0\to K_S\pi^0)$–$\mathcal{B}(D^0\to K_L\pi^0)$ plane which is still allowed by the individual measurements. To quantify our findings further we define

$$R(D^0)\equiv\frac{\mathcal{B}(D^0\to K_S\pi^0)-\mathcal{B}(D^0\to K_L\pi^0)}{\mathcal{B}(D^0\to K_S\pi^0)+\mathcal{B}(D^0\to K_L\pi^0)} \qquad (49)$$

and quote the confidence intervals in the first row of Tab. IX. The ratio of the magnitudes of the DCS and CF amplitudes is listed in the third row of this table. Fig. 9 visualizes these confidence intervals and also shows the prediction of Refs. [52–55], which is the black dot corresponding to $R(D^0)=2\tan^2\theta_C$ (where θ_C is the Cabibbo angle). The result is quoted without uncertainty in these papers and Refs. [53–55] argues that corrections from SU(3) breaking to this relations are small. Refs. [54, 55] arrives at this conclusion by calculating the amplitudes in QCD factorization [56, 57], which is a calculational method valid for values of m_c much larger than the hadronic scale governing the infrared structure of the decays. Our fit permits sizable corrections to $R(D^0)=2\tan^2\theta_C$ from the SU(3) breaking contributions, so that future measurements will give insight into

[1] In order to find the correct relative signs in Eqs. (47) and (48) one must define $K_{S,L}$ correctly. Eqs. (1) and (2) comply with $|K^0\rangle = C\,|\overline{K}^0\rangle = -CP\,|\overline{K}^0\rangle$ entailing $|K_S\rangle\simeq(|K^0\rangle-|\overline{K}^0\rangle)/\sqrt{2}$. We have checked our results by studying the full decay chain $D^0\to{}^{(}\overline{K}^{0)}[\to\pi^+\pi^-]\pi^0$, from which the K^0 sign conventions drop out.

the size of SU(3) breaking and the viability of QCD factorization in charm physics.

Another test of doubly Cabibbo-suppressed contributions involves the decays $D_s^+ \to K_{S,L}K^+$. We study

$$R(D_s^+) \equiv \frac{\mathcal{B}(D_s^+ \to K_S K^+) - \mathcal{B}(D_s^+ \to K_L K^+)}{\mathcal{B}(D_s^+ \to K_S K^+) + \mathcal{B}(D_s^+ \to K_L K^+)} \quad (50)$$

and predict the not yet measured observables $R(D_s^+)$ and $\mathcal{B}(D_s^+ \to K_L K^+)$, see Tab. IX and Fig. 9. Again comparing our result with the prediction in Ref. [55] we find much larger uncertainties. Thus also in $D_s^+ \to K_{S,L}K^+$ future data will test the accuracy of QCD factorization assumed in Ref. [55].

V. CONCLUSION

We have studied the decay amplitudes of D mesons into two pseudoscalar mesons with the topological-amplitude approach. To this end we have incorporated linear $\mathrm{SU}(3)_F$ breaking into the method and have shown that the topological amplitude method can be mapped onto the standard decomposition of the decay amplitudes in terms of reduced amplitudes characterized by $\mathrm{SU}(3)_F$ representations. Unlike plain $\mathrm{SU}(3)_F$ analyses the topological-amplitude method permits the use of a $1/N_c$ expansion to calculate the factorizable tree and annihilation amplitudes in terms of form factors and decay constants, up to corrections of order $1/N_c^2$. This additional theoretical input has lead us to a new sum rule between the branching fractions of $D^+ \to K_S K^+$, $D_s^+ \to K_S \pi^+$ and $D^+ \to K^+ \pi^0$. This sum rule correlates the non-factorizable $1/N_c^2$ terms with the penguin amplitude P_{break}. The latter quantity is of prime interest to understand the dynamics of flavour-changing neutral current transitions in the charm sector, because P_{break} is suppressed by the GIM mechanism and vanishes in the limit $m_s = m_d$.

We have then performed a global fit using all available branching ratios and the experimental information on the strong phase difference $\delta_{K^+\pi^-}$. In our analysis we have included the information on correlations between experimental errors. It is possible to find a perfect fit, with a large parameter region satisfying $\chi^2 = 0$. This means that current data comply with i) the Grossman-Robinson sum rules [29], ii) our chosen upper bound of 50% on $\mathrm{SU}(3)_F$ breaking, and iii) our assumption that the $1/N_c^2$ corrections to the factorizable amplitudes are smaller than 15% of the factorized tree amplitude. The main phenomenological results of our paper are various likelihood ratio tests addressing the sizes of the topological amplitudes and their $\mathrm{SU}(3)_F$ breaking (Tab. VIII and Figs. 3–6). Importantly, we find that there is no evidence for an enhanced broken penguin. The hypothesis $P_{\mathrm{break}} = 0$ is rejected at below 1σ only, i.e., insignificantly. Improvements of $\mathcal{B}(D^+ \to K_S K^+)$, $\mathcal{B}(D_s^+ \to K_S \pi^+)$, $\mathcal{B}(D^+ \to K^+ \pi^0)$ and especially the form factor $F_0^{K\pi}(m^2_{D_{(s)}})$ could advance our knowledge of the GIM mechanism in charm by pinning down the proportions of broken penguin and $1/N_c^2$ corrections. The current status is summarized in Fig. 6(c). While the SCS branching ratios $\mathcal{B}(D^+ \to K_S K^+)$ and $\mathcal{B}(D_s^+ \to K_S \pi^+)$ are known at a precision of $\lesssim 6\%$ the relative uncertainty of the DCS branching ratio $\mathcal{B}(D^+ \to K^+ \pi^0)$ is about $\sim 14\%$ and leaves room for improvement. As the latter is the only charm decay into kaons and pions which depends on factorizable contributions only, it is very important to improve its measurement. With a simultaneously improved $F_0^{K\pi}(m^2_{D_{(s)}})$ the branching ratio $\mathcal{B}(D^+ \to K^+ \pi^0)$ serves as a test of factorization in charm decays.

We observe a slightly larger $\mathrm{SU}(3)_F$ breaking in color-suppressed tree than in exchange diagrams. In no channel more than $\sim 30\%$ $\mathrm{SU}(3)_F$ breaking is needed to describe the data (not considering $D^0 \to K_S K_S$, which is forbidden in the $\mathrm{SU}(3)_F$ limit); this finding agrees with the plain $\mathrm{SU}(3)_F$ analysis of Ref. [23]. However, as a matter of principle one cannot decide whether or not the actual $\mathrm{SU}(3)_F$ breaking is larger than this. This can potentially only be achieved by future QCD calculations on the lattice [58]. In the data, there is no indication of this to be the case.

With our topological-amplitude fit it is further possible to make predictions for branching fractions which can be probed by future measurements. Despite our conservative ranges for the $\mathrm{SU}(3)_F$ breaking parameters, we find a correlation between $\mathcal{B}(D^0 \to K_L \pi^0)$ and $\mathcal{B}(D^0 \to K_S \pi^0)$ probing the doubly Cabibbo-suppressed contributions to these modes: Fig. 8 entails the prediction $\mathcal{B}(D^0 \to K_L \pi^0) < \mathcal{B}(D^0 \to K_S \pi^0)$ at more than 4σ.

Observable	$\pm 1\sigma$	$\pm 2\sigma$	$\pm 3\sigma$
$R(D^0)$	$0.09^{+0.04}_{-0.02}$	$0.09^{+0.07}_{-0.04}$	$0.09^{+0.09}_{-0.05}$
$R(D_s^+)$	$0.11^{+0.04}_{-0.14}$	$0.11^{+0.05}_{-0.18}$	$0.11^{+0.06}_{-0.19}$
$\mathcal{B}(D_s^+ \to K_L K^+)$	$0.012^{+0.004}_{-0.001}$	$0.012^{+0.006}_{-0.002}$	$0.012^{+0.007}_{-0.002}$
$\left\lvert\frac{\mathcal{A}^{\mathrm{DCS}}(D^0\to K^0\pi^0)}{\mathcal{A}^{\mathrm{CF}}(D^0\to \bar{K}^0\pi^0)}\right\rvert$	$0.05^{+0.02}_{-0.01}$	$0.05^{+0.03}_{-0.03}$	$0.05^{+0.04}_{-0.03}$
$\left\lvert\frac{\mathcal{A}^{\mathrm{DCS}}(D_s^+\to K^0K^+)}{\mathcal{A}^{\mathrm{CF}}(D_s^+\to \bar{K}^0K^+)}\right\rvert$	$0.08^{+0.02}_{-0.06}$	$0.08^{+0.03}_{-0.06}$	$0.08^{+0.04}_{-0.07}$

TABLE IX: Fit results for several observables probing doubly Cabibbo-suppressed amplitudes. The corresponding plots are shown in Fig. 9.

Acknowledgments

We thank Philipp Frings, Gudrun Hiller and Martin Jung for useful discussions. The fits are performed using the `python` version of the software package `myFitter` [34]. StS thanks Martin Wiebusch for `myFitter` support and the provision of `myFitter-python-0.2-beta`. The Feynman diagrams are drawn using `Jaxodraw` [59, 60]. The presented work is supported by BMBF under contract no. 05H12VKF.

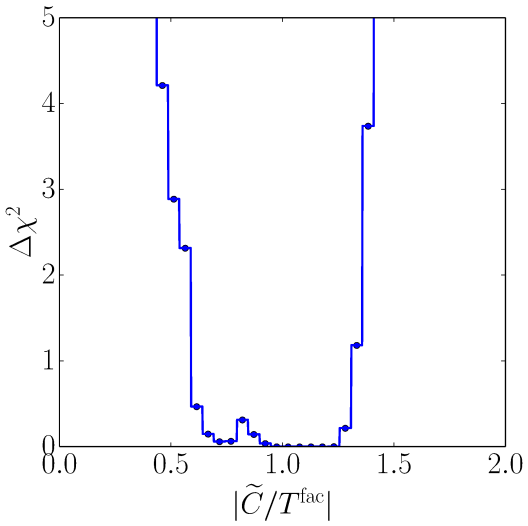

(a)

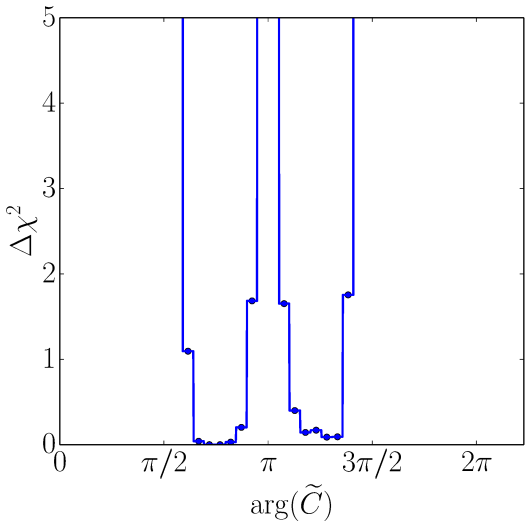

(b)

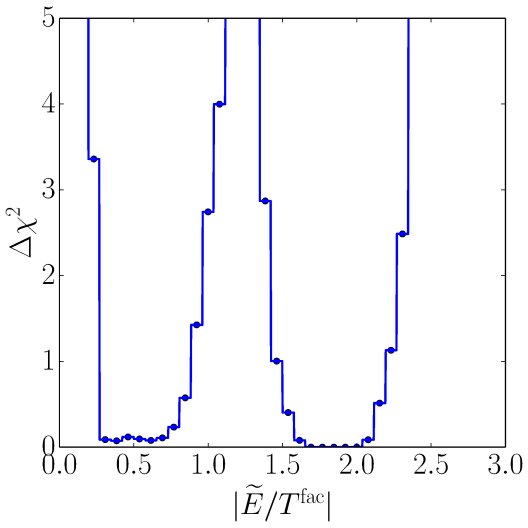

(c)

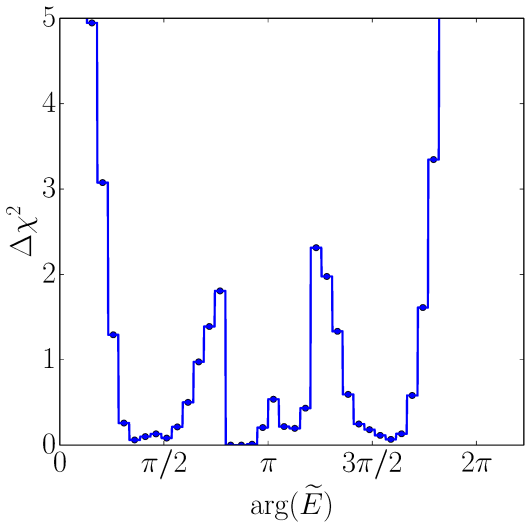

(d)

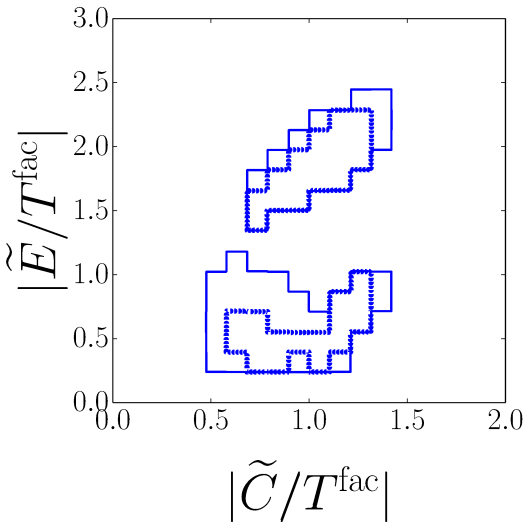

(e)

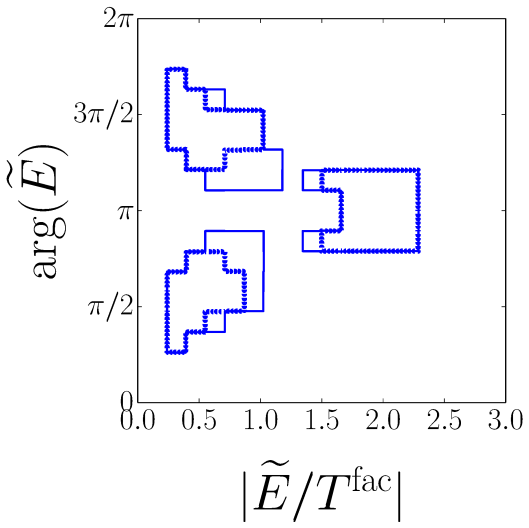

(f)

FIG. 3: SU(3)$_F$ limit topologies. In Figs. (e) and (f) the dashed (solid) line denotes the 68% (95%) C.L. contour.

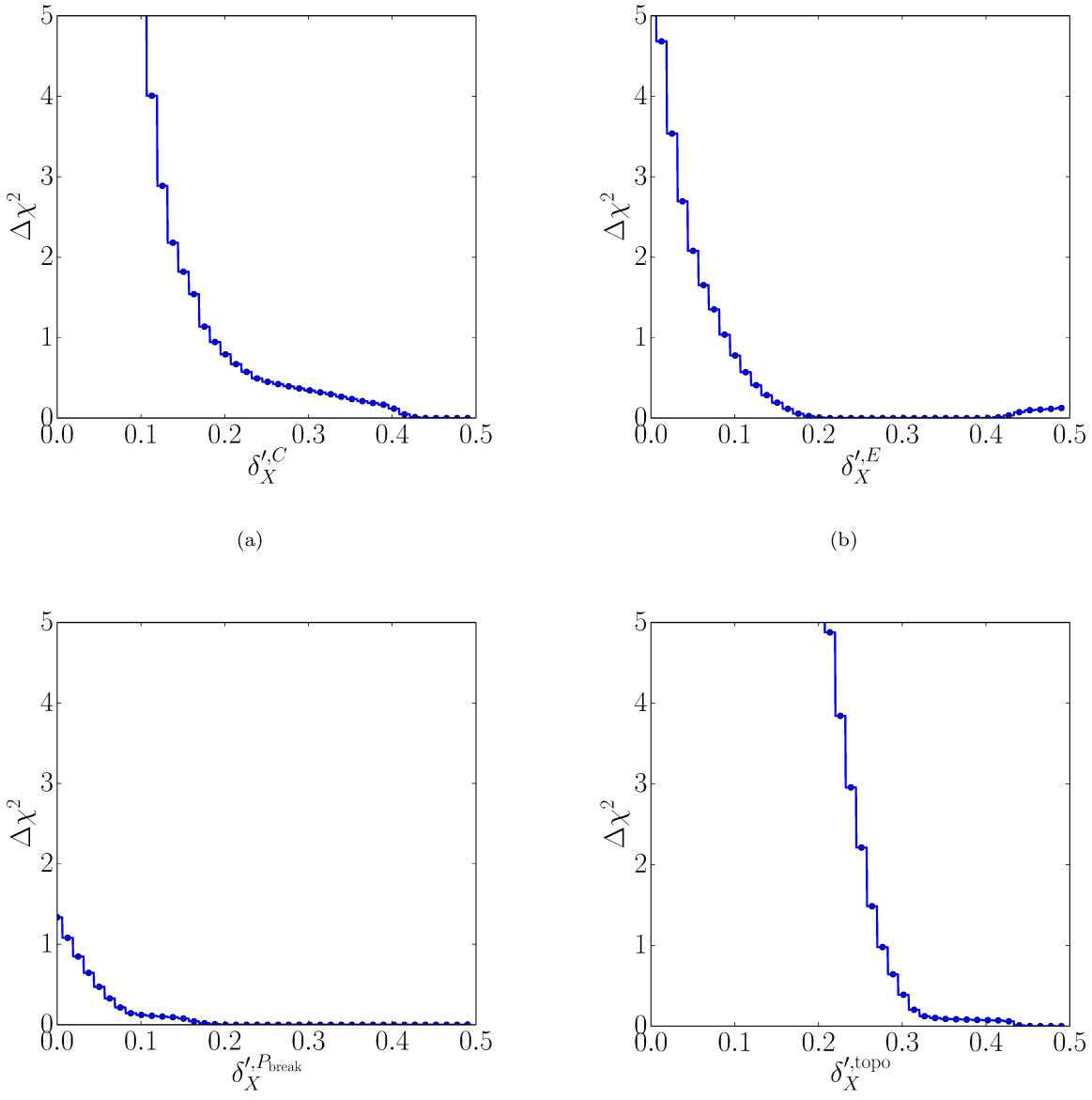

(a) (b)

(c) (d)

FIG. 4: $\Delta\chi^2$ profile of the parameters $\delta_X'^{,C,E,P_{\rm break}}$ measuring SU(3)$_F$-breaking in C, E, and $P_{\rm break}$ (a,b,c) and of $\delta_X'^{,\rm topo}$ defined in Eq. (44), which quantifies the overall SU(3)$_F$-breaking (d).

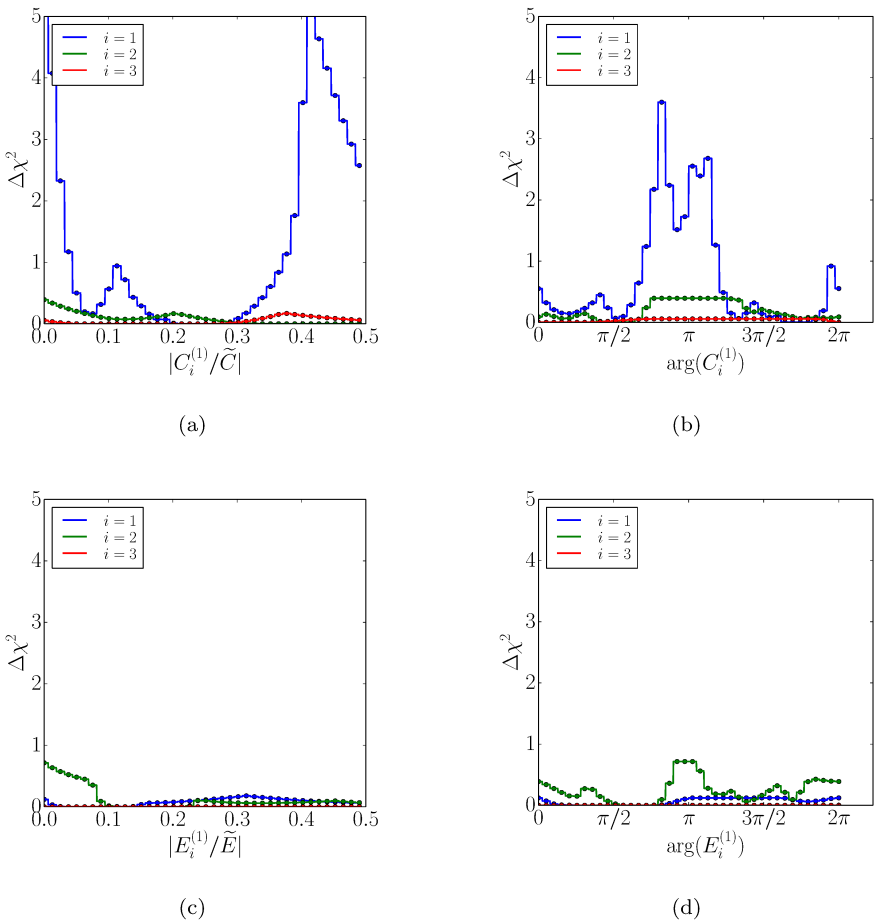

FIG. 5: $SU(3)_F$-breaking color-suppressed tree (a,b) and exchange (c,d) topologies.

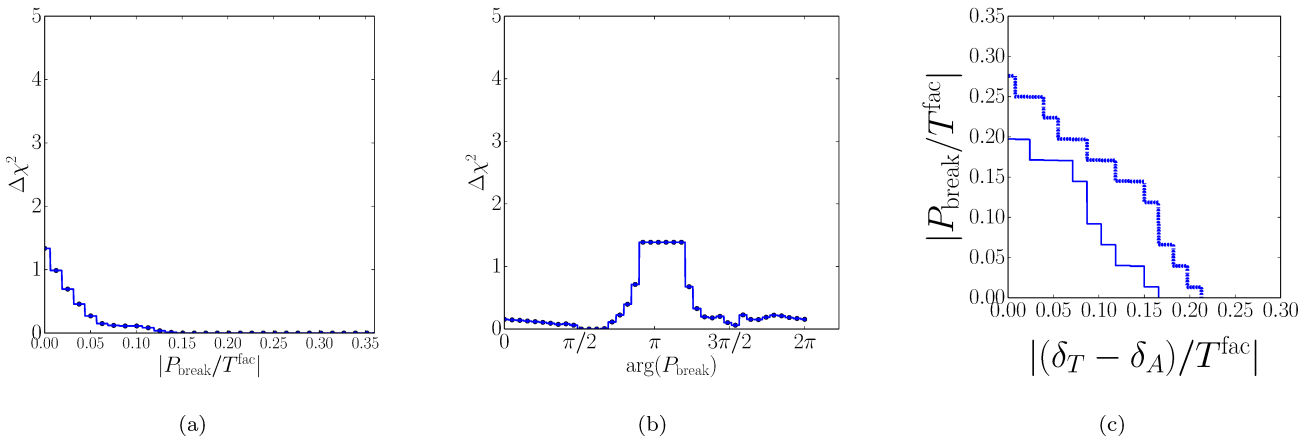

FIG. 6: The broken penguin (a,b) and its correlation to parameters measuring the $1/N_c$ corrections (c). In Fig. (c) the dashed (solid) line denotes the 68% (95%) C.L. contour and the region to the right of the contours is allowed.

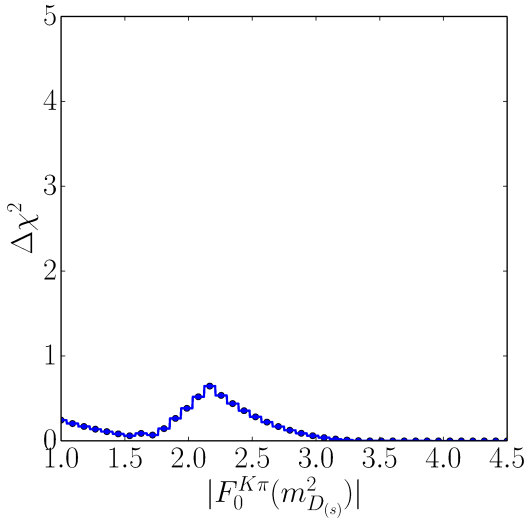

FIG. 7: The form factor $F_0^{K\pi}(m^2_{D_{(s)}})$.

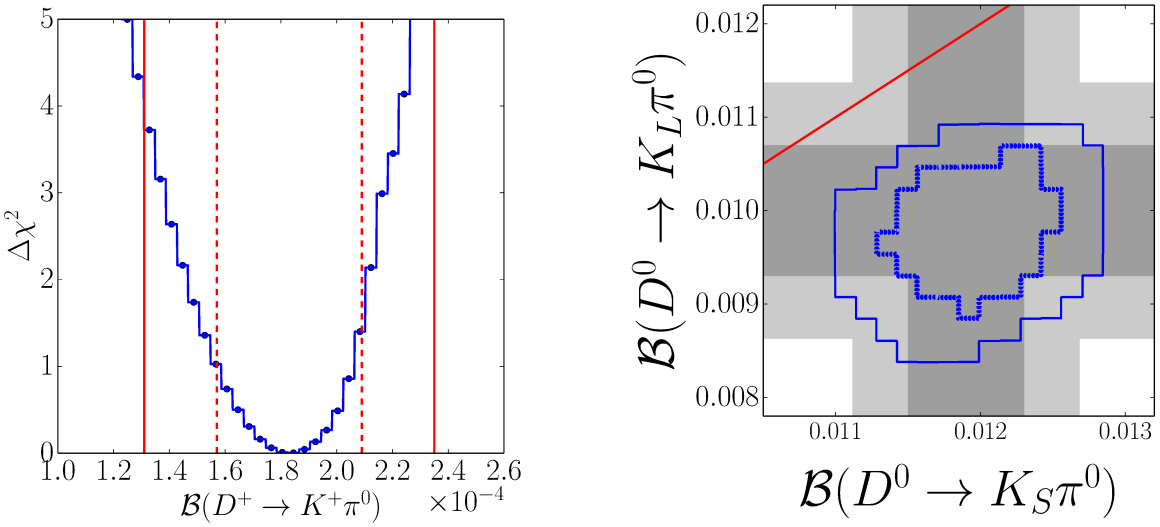

(a) (b)

FIG. 8: $\Delta\chi^2$ profile of $\mathcal{B}(B^+ \to K^+\pi^0)$ (a) and correlation between $\mathcal{B}(D^0 \to K_L\pi^0)$ and $\mathcal{B}(D^0 \to K_S\pi^0)$ (b). In Fig. (a) the red dashed (solid) line indicates the 1σ (2σ) experimental error. In Fig. (b) the dashed (solid) lines are the 68% (95%) C.L. contours of our fit and the dark (light) gray shading denotes the 68% (95%) C.L. region of the measurements. Here, the solid red line corresponds to $\mathcal{B}(D^0 \to K_L\pi^0) = \mathcal{B}(D^0 \to K_S\pi^0)$.

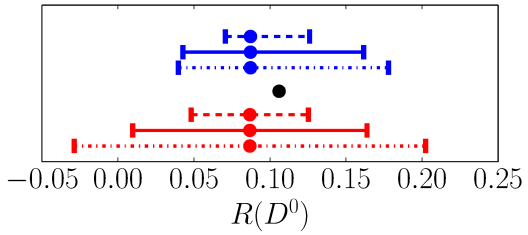

(a) Black: prediction of Refs. [52–55]. Red (below the black point): experimental error

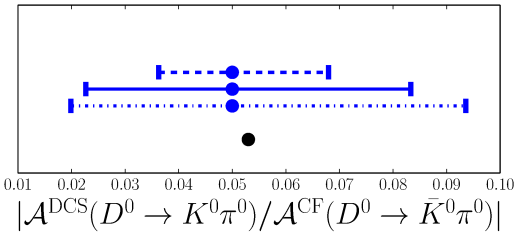

(b) Black: prediction of Refs. [52–55]

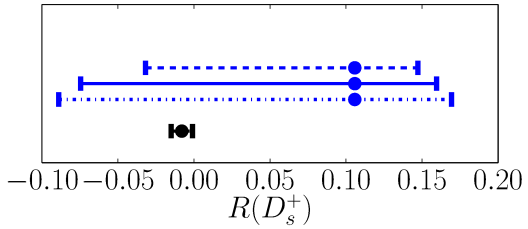

(c) Black: 1σ range predicted in Ref. [55]

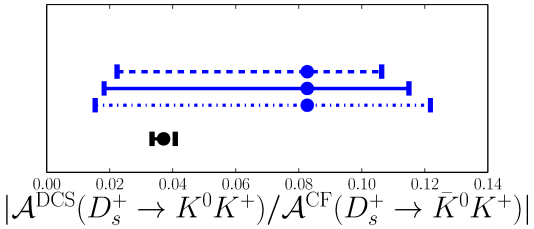

(d) Black: 1σ range predicted in Ref. [55]

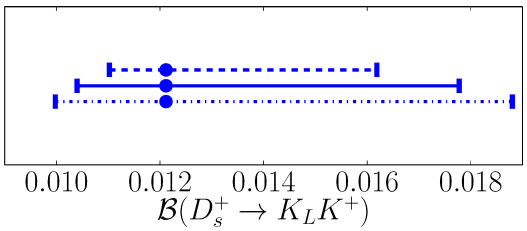

(e)

FIG. 9: Blue: Our results for several observables probing doubly Cabibbo-suppressed amplitudes (see Eqs. (49) and (50)). The lines correspond to 1σ (dashed), 2σ (solid) and 3σ (dashed-dotted) confidence intervals, respectively. The experimental error in $R(D^0)$ is obtained by Gaussian error propagation from Tab. X. The results from other groups [52–55] are shown in black. In case of $R(D^0)$ (a) and $\left|\frac{\mathcal{A}^{\rm DCS}(D^0\to K^0\pi^0)}{\mathcal{A}^{\rm CF}(D^0\to \bar{K}^0\pi^0)}\right|$ (b) no errors are given in Refs. [52–55].

Observable	Measurement	References
SCS branching ratios		
$\mathcal{B}(D^0 \to K^+K^-)$	$(3.96 \pm 0.08) \cdot 10^{-3}$	[46]
$\mathcal{B}(D^0 \to \pi^+\pi^-)$	$(1.402 \pm 0.026) \cdot 10^{-3}$	[46]
$\mathcal{B}(D^0 \to K_S K_S)$	$(0.17 \pm 0.04) \cdot 10^{-3}$	[46]
$\mathcal{B}(D^0 \to \pi^0\pi^0)$	$(0.820 \pm 0.035) \cdot 10^{-3}$	[46]
$\mathcal{B}(D^+ \to \pi^0\pi^+)$	$(1.19 \pm 0.06) \cdot 10^{-3}$	[46]
$\mathcal{B}(D^+ \to K_S K^+)$	$(2.83 \pm 0.16) \cdot 10^{-3}$	[46]
$\mathcal{B}(D_s^+ \to K_S\pi^+)/\mathcal{B}(D_s^+ \to K_S K^+)$	$(8.12 \pm 0.28) \cdot 10^{-2}$	[46]
$\mathcal{B}(D_s^+ \to K^+\pi^0)/\mathcal{B}(D_s^+ \to K_S K^+)$	$(4.2 \pm 1.4) \cdot 10^{-2}$	[46]
CF branching ratios		
$\mathcal{B}(D^0 \to K^-\pi^+)$	$(3.88 \pm 0.05) \cdot 10^{-2}$	[46]
$\mathcal{B}(D^0 \to K_S\pi^0)$	$(1.19 \pm 0.04) \cdot 10^{-2}$	[46]
$\mathcal{B}(D^0 \to K_L\pi^0)$	$(1.00 \pm 0.07) \cdot 10^{-2}$	[46]
$\mathcal{B}(D^+ \to K_S\pi^+)$	$(1.47 \pm 0.07) \cdot 10^{-2}$	[46]
$\mathcal{B}(D^+ \to K_L\pi^+)$	$(1.46 \pm 0.05) \cdot 10^{-2}$	[46]
$\mathcal{B}(D_s^+ \to K_S K^+)$	$(1.50 \pm 0.05) \cdot 10^{-2}$	†[47, 48]
DCS branching ratios		
$\mathcal{B}(D^0 \to K^+\pi^-)/\mathcal{B}(D^0 \to K^-\pi^+)$	0.00349 ± 0.00004	[61]
$\mathcal{B}(D^+ \to K^+\pi^0)$	$(1.83 \pm 0.26) \cdot 10^{-4}$	[46]
$K^+\pi^-$ strong phase difference		
$\delta_{K\pi}$	$(6.45 \pm 10.65)^\circ$	‡[61]

TABLE X: Input data for charm meson branching ratios and the strong phase difference $\delta_{K\pi}$ used in our fit. Note that as we incorporate the correlations reported in Ref. [46], for consistency we do not take into account the experimental updates of the following branching fractions: $\mathcal{B}(D^0 \to K^-\pi^+)$ [62] and $\mathcal{B}(D^+ \to K_S\pi^+)$ [62]. For the correlation coefficients see Tabs. XI, XII and XIII. Note that $\mathcal{B}(D_s^+ \to K^+\pi^0)$ and $\mathcal{B}(D_s^+ \to K_S\pi^+)$ are not part of the PDG fit, i.e., there are no correlation coefficients given for these decay modes. We therefore have no correlation matrix for D_s^+ decays. The value for $\mathcal{B}(D^0 \to K^+\pi^-)/\mathcal{B}(D^0 \to K^-\pi^+)$ is taken from the Heavy Flavor Averaging Group (HFAG) in order to take its correlation with $\delta_{K\pi}$ into account, see Tab. XIII. †Our average. ‡Our symmetrization of uncertainties.

	$\mathcal{B}_{D^0}^{K^+K^-}$	$\mathcal{B}_{D^0}^{\pi^+\pi^-}$	$\mathcal{B}_{D^0}^{K_SK_S}$	$\mathcal{B}_{D^0}^{\pi^0\pi^0}$	$\mathcal{B}_{D^0}^{K^-\pi^+}$	$\mathcal{B}_{D^0}^{K_S\pi^0}$
$\mathcal{B}_{D^0}^{K^+K^-}$	1.00	0.38	0.03	0.09	0.60	0.21
$\mathcal{B}_{D^0}^{\pi^+\pi^-}$	0.38	1.00	0.03	0.09	0.62	0.22
$\mathcal{B}_{D^0}^{K_SK_S}$	0.03	0.03	1.00	0.01	0.05	0.03
$\mathcal{B}_{D^0}^{\pi^0\pi^0}$	0.09	0.09	0.01	1.00	0.14	0.05
$\mathcal{B}_{D^0}^{K^-\pi^+}$	0.60	0.62	0.05	0.14	1.00	0.35
$\mathcal{B}_{D^0}^{K_S\pi^0}$	0.21	0.22	0.03	0.05	0.35	1.00

TABLE XI: Correlation coefficients for D^0 branching ratios [46] used in our fit. We abbreviate $\mathcal{B}_i^f \equiv \mathcal{B}(i \to f)$. Note that $\mathcal{B}(D^0 \to K_L\pi^0)$ is not part of the PDG fit and used without correlations to the other modes.

	$\mathcal{B}_{D^+}^{K_SK^+}$	$\mathcal{B}_{D^+}^{K_S\pi^+}$	$\mathcal{B}_{D^+}^{K^+\pi^0}$
$\mathcal{B}_{D^+}^{K_SK^+}$	1.00	0.75	0.05
$\mathcal{B}_{D^+}^{K_S\pi^+}$	0.75	1.00	0.06
$\mathcal{B}_{D^+}^{K^+\pi^0}$	0.05	0.06	1.00

TABLE XII: Correlation coefficients for D^+ branching ratios [46] used in our fit, see the caption of Tab. XI for the used notation. Note that $\mathcal{B}(D^+ \to K_L\pi^+)$ and $\mathcal{B}(D^+ \to \pi^0\pi^+)$ are not part of the PDG fit and used without correlations to the other modes.

Appendix A: Input Data

We give the input data used in the fits, including the correlation coefficients, in Tabs. X–XIV. For details on the input values for the form factors see Appendices C 1 and C 2.

Appendix B: Mapping of the topological on the SU(3)$_F$ parameterization

As discussed in Sec. II C the topological flavor-flow parameterization and the linear SU(3)$_F$ expansion can be mapped onto each other after the removal of redundancies in each parameterization. Both redundant parameters and redundant decay amplitudes have to be removed in order to obtain two corresponding 11×11 regular coefficient matrices. Then, the mapping can be calculated by inverting one or the other coefficient matrix. We choose to omit the redundant amplitudes

$$D^0 \to \pi^0\pi^0\,, \quad D^0 \to K^-\pi^+\,, \quad D^0 \to K^+\pi^-\,, \tag{B1}$$

$$D^0 \to K^0\pi^0\,, \quad D^+ \to K^0\pi^+\,, \quad D^+ \to K^+\pi^0\,, \tag{B2}$$

using the sum rules presented in Sec. D. We next calculate the redefined SU(3)$_F$ matrix elements in terms of the remaining decay amplitudes by inverting the SU(3)$_F$ coefficient matrix given in Tabs. I and V of Ref. [23] The result for this inverse matrix is given in Tab. XVII. In order to illustrate how to read Tab. XVII, we exemplify

$$A_{27}^{15} = \frac{2\sqrt{2}}{3}\mathcal{A}(D^+ \to \bar{K}^0\pi^+) + \frac{\sqrt{2}}{3}\mathcal{A}(D_s^+ \to K^0K^+)\,. \tag{B3}$$

Inserting the expansions of $\mathcal{A}(D^+ \to \bar{K}^0\pi^+)$ and $\mathcal{A}(D_s^+ \to K^0K^+)$ in terms of topological amplitudes into Eq. (B3) gives the desired expression of the SU(3)$_F$ matrix element A_{27}^{15} in terms of the topological amplitudes. In Tabs. XV and XVI we give two numerical examples for the mapping. Note that in the matching we implicitly disregard higher order SU(3)$_F$-breaking effects which are included in the approximate factorization formulas. Strictly speaking, these invalidate the linear SU(3)$_F$ sum rules, see also Sec. III A. However, this can be safely neglected as we only aim at a description of the data at linear SU(3)$_F$ breaking here.

While the exemplified topological-amplitude fit points respect the SU(3)$_F$ power counting, the SU(3)$_F$ breaking matrix elements can nevertheless be quite large, like

	$\delta_{K\pi}$	$\frac{\mathcal{B}(D^0\to K^+\pi^-)}{\mathcal{B}(D^0\to K^-\pi^+)}$
$\delta_{K\pi}$	1.000	0.404
$\frac{\mathcal{B}(D^0\to K^+\pi^-)}{\mathcal{B}(D^0\to K^-\pi^+)}$	0.404	1.000

TABLE XIII: Correlation between $\mathcal{B}(D^0\to K^+\pi^-)/\mathcal{B}(D^0\to K^-\pi^+)$ and $\delta_{K\pi}$ [61] used in our fit.

$F_0^{DK}(0)$	0.737 ± 0.005	†[63–67]
$F_0^{D\pi}(0)$	0.638 ± 0.012	†[63–66]
$F_0^{D_sK}(0)$	$(1 \pm 5\%) \times F_0^{D\pi}(0)$	[68, 69]

TABLE XIV: Numerical input for the form factors. The form factor $F_0^{D_sK}(0)$ is varied flatly within the theory uncertainty [70]. Table adapted from [71]. †Our average.

$|\widetilde{B}_1^3| \sim 0.7$ in Tab. XV in case of example point I. This shows that several small $\mathrm{SU}(3)_F$ breaking parameters of the topological-amplitude fit can add up to a larger $\mathrm{SU}(3)_F$ breaking matrix element of the group-theoretical approach. However, as demonstrated by the example point II in Tab. XVI, there are also solutions where both diagrammatic and group theoretic language give $\mathrm{SU}(3)_F$ breaking $\lesssim 50\%$.

Appendix C: Approximate factorization formulas

Below, we give the $1/N_c$-leading expressions for the tree and annihilation diagrams. Corrections of higher order in the $1/N_c$-expansion are parameterized by δ_T and δ_A introduced in Sec. III A.

1. Factorization of tree amplitudes

We use the following expressions for the $1/N_c$-leading contributions to the tree diagrams. $\mathrm{SU}(3)_F$ breaking in the $1/N_c^2$ corrections is of higher order in our power counting and neglected, i.e., we use a flavor-universal correction parameter δ_T. In our fit we vary

$$0 \le |\delta_T| \le 0.15\, T^{\mathrm{fac}}\,, \tag{C1}$$

$$0 \le \arg(\delta_T) \le 2\pi\,, \tag{C2}$$

with T^{fac} defined in Eq. (24) and $\delta_T = T - T^{\mathrm{fac}}$, see Eq. (23). The $1/N_c$-leading, factorizable contributions to the SCS tree amplitudes are altogether given as:

$$T^{\mathrm{fac}}_{D^0\to K^+K^-} = \frac{G_F}{\sqrt{2}} a_1 f_K (m_D^2 - m_K^2) F_0^{DK}(m_K^2)\,, \tag{C3}$$

$$T^{\mathrm{fac}}_{D^0\to \pi^+\pi^-} = -\frac{G_F}{\sqrt{2}} a_1 f_\pi (m_D^2 - m_\pi^2) F_0^{D\pi}(m_\pi^2)\,, \tag{C4}$$

$$T^{\mathrm{fac}}_{D^+\to \pi^+\pi^0} = -\frac{G_F}{\sqrt{2}}\frac{1}{\sqrt{2}} a_1 f_\pi (m_D^2 - m_\pi^2) F_0^{D\pi}(m_\pi^2)\,, \tag{C5}$$

Topological parameter	value	$\mathrm{SU}(3)_F$ matrix element	value
$\lvert\delta_A\rvert/T^{\mathrm{fac}}$	0.14	$\lvert\widetilde{A}_{27}^{15}\rvert$	0.32
$\lvert\delta_T\rvert/T^{\mathrm{fac}}$	0.15	$\lvert\widetilde{A}_{8}^{15}\rvert$	0.22
$\arg(\delta_A/T^{\mathrm{fac}})$	0.17	$\lvert\widetilde{A}_{8}^{\bar{6}}\rvert$	1.00
$\arg(\delta_T/T^{\mathrm{fac}})$	3.22	$\lvert\widetilde{B}_{1}^{3}\rvert$	0.67
$\lvert F_0^{K\pi}(m^2_{D_{(s)}})\rvert$	3.54	$\lvert\widetilde{B}_{8}^{3}\rvert$	0.22
$F_0^{DK}(0)$	0.74	$\lvert\widetilde{B}_{8}^{\bar{6}_1}\rvert$	0.36
$F_0^{D\pi}(0)$	0.64	$\lvert\widetilde{B}_{8}^{15_1}\rvert$	0.39
$F_0^{D_sK}(0)/F_0^{D\pi}(0)$	0.95	$\lvert\widetilde{B}_{8}^{15_2}\rvert$	0.29
$\arg(F_0^{K\pi}(m^2_{D_{(s)}}))$	4.54	$\lvert\widetilde{B}_{27}^{15_1}\rvert$	0.18
$\lvert\widetilde{C}/T^{\mathrm{fac}}\rvert$	1.10	$\lvert\widetilde{B}_{27}^{15_2}\rvert$	0.07
$\lvert\widetilde{E}/T^{\mathrm{fac}}\rvert$	0.46	$\lvert\widetilde{B}_{27}^{24_1}\rvert$	0.13
$\lvert P_{\mathrm{break}}/T^{\mathrm{fac}}\rvert$	0.05	$\arg(A_{27}^{15})$	1.44
$\arg(\widetilde{C})$	2.47	$\arg(A_{8}^{15})$	−2.53
$\arg(C_1^{(1)})$	4.78	$\arg(A_{8}^{\bar{6}})$	0.20
$\arg(C_2^{(1)})$	4.88	$\arg(B_{1}^{3})$	−0.53
$\arg(C_3^{(1)})$	0.00	$\arg(B_{8}^{3})$	−0.96
$\arg(\widetilde{E})$	1.49	$\arg(B_{8}^{\bar{6}_1})$	−2.11
$\arg(E_1^{(1)})$	5.63	$\arg(B_{8}^{15_1})$	−1.35
$\arg(E_2^{(1)})$	5.36	$\arg(B_{8}^{15_2})$	−2.30
$\arg(E_3^{(1)})$	5.13	$\arg(B_{27}^{15_1})$	2.56
$\arg(P_{\mathrm{break}})$	0.18	$\arg(B_{27}^{15_2})$	3.10
$\lvert C_1^{(1)}/\widetilde{C}\rvert$	0.07	$\arg(B_{27}^{24_1})$	0.00
$\lvert C_2^{(1)}/\widetilde{C}\rvert$	0.16		
$\lvert C_3^{(1)}/\widetilde{C}\rvert$	0.19		
$\lvert E_1^{(1)}/\widetilde{E}\rvert$	0.50		
$\lvert E_2^{(1)}/\widetilde{E}\rvert$	0.50		
$\lvert E_3^{(1)}/\widetilde{E}\rvert$	0.05		
$\delta_X^{\prime,\mathrm{topo}}$	0.50		
$\delta_X^{\prime,C}$	0.50		
$\delta_X^{\prime,E}$	0.31		
$\delta_X^{\prime,P_{\mathrm{break}}}$	0.07		
χ^2	0.27		

TABLE XV: Fit example point I and corresponding point in the $\mathrm{SU}(3)_F$ decomposition with linear $\mathrm{SU}(3)_F$ breaking. The values quoted for $\widetilde{A}_j^i$ and $\widetilde{B}_j^i$ in the last column are normalized to the largest $\mathrm{SU}(3)_F$ limit matrix element. The fit is only sensitive to δ_T and δ_A in the combination $(\delta_T - \delta_A)/T^{\mathrm{fac}} = 0.29e^{-3.02\,i}$.

$$T^{\mathrm{fac}}_{D^+\to K^+\bar{K}^0} = \frac{G_F}{\sqrt{2}} a_1 f_K (m_D^2 - m_K^2) F_0^{DK}(m_K^2)\,, \tag{C6}$$

$$T^{\mathrm{fac}}_{D_s^+\to \pi^+K^0} = -\frac{G_F}{\sqrt{2}} a_1 f_\pi (m_{D_s}^2 - m_K^2) F_0^{D_sK}(m_\pi^2). \tag{C7}$$

The $1/N_c$-leading, factorizable contributions to the CF tree amplitudes are given as:

$$T^{\mathrm{fac}}_{D^0\to K^-\pi^+} = \frac{G_F}{\sqrt{2}} a_1 f_\pi (m_D^2 - m_K^2) F_0^{DK}(m_\pi^2)\,, \tag{C8}$$

Topological parameter	value	$SU(3)_F$ matrix element	value
$\lvert\delta_A\rvert/T^{\rm fac}$	0.15	$\lvert\widetilde{A}_{27}^{15}\rvert$	0.35
$\lvert\delta_T\rvert/T^{\rm fac}$	0.15	$\lvert\widetilde{A}_{8}^{15}\rvert$	1.00
$\arg(\delta_A/T^{\rm fac})$	1.27	$\lvert\widetilde{A}_{8}^{\bar{6}}\rvert$	0.19
$\arg(\delta_T/T^{\rm fac})$	4.40	$\lvert\widetilde{B}_{1}^{3}\rvert$	0.36
$\lvert F_0^{K\pi}(m^2_{D_{(s)}})\rvert$	4.50	$\lvert\widetilde{B}_{8}^{3}\rvert$	0.10
$F_0^{DK}(0)$	0.74	$\lvert\widetilde{B}_{8}^{\bar{6}_1}\rvert$	0.15
$F_0^{D\pi}(0)$	0.64	$\lvert\widetilde{B}_{8}^{15_1}\rvert$	0.49
$F_0^{D_sK}(0)/F_0^{D\pi}(0)$	0.95	$\lvert\widetilde{B}_{8}^{15_2}\rvert$	0.06
$\arg(F_0^{K\pi}(m^2_{D_{(s)}}))$	4.78	$\lvert\widetilde{B}_{27}^{15_1}\rvert$	0.17
$\lvert\widetilde{C}/T^{\rm fac}\rvert$	1.17	$\lvert\widetilde{B}_{27}^{15_2}\rvert$	0.21
$\lvert\widetilde{E}/T^{\rm fac}\rvert$	2.05	$\lvert\widetilde{B}_{27}^{24_1}\rvert$	0.06
$\lvert P_{\rm break}/T^{\rm fac}\rvert$	0.39	$\arg(A_{27}^{15})$	0.94
$\arg(\widetilde{C})$	2.23	$\arg(A_{8}^{15})$	−0.60
$\arg(C_1^{(1)})$	5.22	$\arg(A_{8}^{\bar{6}})$	1.47
$\arg(C_2^{(1)})$	1.48	$\arg(B_{1}^{3})$	2.15
$\arg(C_3^{(1)})$	0.22	$\arg(B_{8}^{3})$	0.55
$\arg(\widetilde{E})$	2.57	$\arg(B_{8}^{\bar{6}_1})$	−2.04
$\arg(E_1^{(1)})$	0.23	$\arg(B_{8}^{15_1})$	−2.00
$\arg(E_2^{(1)})$	1.72	$\arg(B_{8}^{15_2})$	−1.25
$\arg(E_3^{(1)})$	0.75	$\arg(B_{27}^{15_1})$	−2.84
$\arg(P_{\rm break})$	1.97	$\arg(B_{27}^{15_2})$	−1.53
$\lvert C_1^{(1)}/\widetilde{C}\rvert$	0.22	$\arg(B_{27}^{24_1})$	0.23
$\lvert C_2^{(1)}/\widetilde{C}\rvert$	0.38		
$\lvert C_3^{(1)}/\widetilde{C}\rvert$	0.12		
$\lvert E_1^{(1)}/\widetilde{E}\rvert$	0.06		
$\lvert E_2^{(1)}/\widetilde{E}\rvert$	0.09		
$\lvert E_3^{(1)}/\widetilde{E}\rvert$	0.31		
$\delta_X^{\prime,\rm topo}$	0.50		
$\delta_X^{\prime,C}$	0.50		
$\delta_X^{\prime,E}$	0.16		
$\delta_X^{\prime,P_{\rm break}}$	0.50		
χ^2	0.12		

TABLE XVI: Fit example point II and corresponding point in the $SU(3)_F$ decomposition with linear $SU(3)_F$ breaking. Cf. Tab. XV for the notation. The fit is only sensitive to δ_T and δ_A in the combination $(\delta_T-\delta_A)/T^{\rm fac}=0.30e^{-1.88\,i}$.

$$T^{\rm fac}_{D^+\to\bar{K}^0\pi^+}=\frac{G_F}{\sqrt{2}}a_1 f_\pi(m_D^2-m_K^2)F_0^{DK}(m_\pi^2). \tag{C9}$$

The $1/N_c$-leading, factorizable contributions to the DCS tree amplitudes are given as:

$$T^{\rm fac}_{D^0\to K^+\pi^-}=\frac{G_F}{\sqrt{2}}a_1 f_K(m_D^2-m_\pi^2)F_0^{D\pi}(m_K^2)\,, \tag{C10}$$

$$T^{\rm fac}_{D^+\to K^+\pi^0}=\frac{G_F}{\sqrt{2}}\frac{1}{\sqrt{2}}a_1 f_K(m_D^2-m_\pi^2)F_0^{D\pi}(m_K^2)\,, \tag{C11}$$

$$T^{\rm fac}_{D_s^+\to K^0K^+}=\frac{G_F}{\sqrt{2}}a_1 f_K(m_{D_s}^2-m_K^2)F_0^{D_sK}(m_K^2). \tag{C12}$$

The matrix element of the vector current can be parameterized by the vector and scalar form factor as [69]

$$\begin{aligned}\langle P|\,V^\mu\,|D\rangle &= F_+^{D\to P}(q^2)\left[p_D^\mu+p_P^\mu-\frac{m_D^2-m_K^2}{q^2}q^\mu\right]\\ &\quad+F_0^{D\to K}(q^2)\frac{m_D^2-m_K^2}{q^2}q^\mu\,,\end{aligned} \tag{C13}$$

with the vector form factor $F_+^{D\to P}$ and the scalar form factor $F_0^{D\to K}$ obeying [69]

$$\langle P|\,S\,|D\rangle = F_0^{D\to P}(q^2)\frac{m_D^2-m_P^2}{m_c-m_p}. \tag{C14}$$

Here the same renormalization scheme and scale must be used for S and m_c-m_p.

We calculate the form factors that appear in the tree amplitudes using the overall scaling factor appearing in the z-parameterization, i.e., a pole factor [69, 72]

$$F_0^{DK}(m_P^2)=\frac{F_0^{DK}(0)}{1-m_P^2/m^2_{D_{s0}^*}(2317)^\pm}\,, \tag{C15}$$

$$F_0^{D_sK}(m_P^2)=\frac{F_0^{D_sK}(0)}{1-m_P^2/m^2_{D_0^*}(2400)^\pm}\,, \tag{C16}$$

$$F_0^{D\pi}(m_P^2)=\frac{F_0^{D\pi}(0)}{1-m_P^2/m^2_{D_0^*}(2400)^\pm}\,, \tag{C17}$$

with the scalar resonances [46]

$$m_{D_{s0}^*}(2317)^\pm=(2317.8\pm0.6)\,\text{MeV}\,, \tag{C18}$$

$$m_{D_0^*}(2400)^\pm=(2403\pm40)\,\text{MeV}. \tag{C19}$$

The used input values for $F_0^{DK}(0)$, $F_0^{D_sK}(0)$ and $F_0^{D\pi}(0)$ are given in Tab. XIV.

As we assume isospin symmetry in the topological-amplitude decomposition we ignore the smallish isospin breaking between charged and neutral masses of kaons and pions for consistency. We use the neutral masses in all amplitudes. However, in the phase space factors of the branching ratios we take the isospin mass splittings into account.

2. Factorization of annihilation amplitudes

We use the following expressions for the $1/N_c$-leading contributions to the annihilation diagrams. As in the case of tree amplitudes we vary δ_A of Eq. (25) as

$$0\le|\delta_A|\le0.15\,T^{\rm fac}\,, \tag{C20}$$

$$0\le\arg(\delta_A)\le2\pi\,. \tag{C21}$$

The $1/N_c$-leading, factorizable contributions [33] to the SCS annihilation amplitudes are given as:

$$A^{\rm fac}_{D^+\to\bar K^0K^+} = 0\,, \tag{C22}$$

$$A^{\rm fac}_{D_s^+\to K^0\pi^+} = \frac{G_F}{\sqrt{2}} a_1 f_{D_s} F_0^{K\pi}(m^2_{D_s}) \left(m_K^2 - m_\pi^2\right)\,, \tag{C23}$$

$$A^{\rm fac}_{D_s^+\to K^+\pi^0} = -\frac{G_F}{\sqrt{2}}\frac{1}{\sqrt{2}} a_1 f_{D_s} F_0^{K\pi}(m^2_{D_s}) \left(m_K^2 - m_\pi^2\right)\,. \tag{C24}$$

The $1/N_c$-leading, factorizable contribution to the CF annihilation amplitude is given as:

$$A^{\rm fac}_{D_s^+\to\bar K^0K^+} = 0\,. \tag{C25}$$

The $1/N_c$-leading, factorizable contributions to the DCS annihilation amplitudes are given as:

$$A^{\rm fac}_{D^+\to K^0\pi^+} = \frac{G_F}{\sqrt{2}} a_1 f_{D} F_0^{K\pi}(m^2_{D}) \left(m_K^2 - m_\pi^2\right)\,, \tag{C26}$$

$$A^{\rm fac}_{D^+\to K^+\pi^0} = -\frac{G_F}{\sqrt{2}}\frac{1}{\sqrt{2}} a_1 f_{D} F_0^{K\pi}(m^2_{D}) \left(m_K^2 - m_\pi^2\right)\,. \tag{C27}$$

Note that the $1/N_c$-leading SCS annihilation amplitude $A^{\rm fac}_{D^+\to\bar K^0K^+}$ and the $1/N_c$-leading CF annihilation amplitude $A^{\rm fac}_{D_s^+\to\bar K^0K^+}$ can be neglected due to isospin symmetry [73]. However, the corresponding $1/N_c^2$ corrections are of course taken into account (as for the others) and specified in Tab. VI.

Constraints on $|F_0^{K\pi}(m^2_{D_{(s)}})|$ can be taken from τ decays. In order to accommodate the measurements of $\tau\to K_S\pi^-\nu_\tau$ from Belle [49] we vary the form factor in the interval

$$1 \lesssim |F_0^{K\pi}(m^2_{D_{(s)}})| \lesssim 4.5\,, \tag{C28}$$

$$0 \lesssim \arg\left(F_0^{K\pi}(m^2_{D_{(s)}})\right) \lesssim 2\pi\,, \tag{C29}$$

setting

$$F_0^{K\pi}(m^2_{D_s}) = F_0^{K\pi}(m^2_{D})\,. \tag{C30}$$

Appendix D: Diagrammatic representation of sum rules

In Tabs. XVIII–XXIII we give the diagrammatic representation of the six Grossman-Robinson $\mathrm{SU}(3)_F$ sum rules which hold to linear order in $\mathrm{SU}(3)_F$ breaking [29].

ME / $\mathcal{A}$	$D^0 \to K^+K^-$	$D^0 \to \pi^+\pi^-$	$D^0 \to \bar{K}^0K^0$	$D^+ \to \pi^0\pi^+$	$D^+ \to \bar{K}^0K^+$	$D_s^+ \to K^0\pi^+$	$D_s^+ \to K^+\pi^0$	$D^0 \to \bar{K}^0\pi^0$	$D^+ \to \bar{K}^0\pi^+$	$D_s^+ \to \bar{K}^0K^+$	$D_s^+ \to K^0K^+$
A_{27}^{15}	0	0	0	0	0	0	0	0	$\frac{2\sqrt{2}}{3}$	0	$\frac{\sqrt{2}}{3}$
A_8^{15}	$-\frac{5}{6\sqrt{2}}$	$\frac{5}{6\sqrt{2}}$	0	0	$\frac{5}{6\sqrt{2}}$	$-\frac{5}{6\sqrt{2}}$	0	$\frac{5}{6}$	$-\frac{1}{3\sqrt{2}}$	$-\frac{5}{6\sqrt{2}}$	$-\frac{1}{6\sqrt{2}}$
$A_8^{\bar{6}}$	$\frac{\sqrt{5}}{2}$	$-\frac{\sqrt{5}}{2}$	0	0	$\frac{\sqrt{5}}{2}$	$-\frac{\sqrt{5}}{2}$	0	$\sqrt{\frac{5}{2}}$	$-\sqrt{5}$	$\frac{\sqrt{5}}{2}$	$-\frac{\sqrt{5}}{2}$
B_1^3	$\frac{16\sqrt{\frac{35}{421}}}{3}$	$\frac{16\sqrt{\frac{35}{421}}}{3}$	$-\frac{16\sqrt{\frac{35}{421}}}{3}$	$-\frac{10\sqrt{\frac{70}{421}}}{3}$	0	$\frac{2\sqrt{\frac{35}{421}}}{3}$	$\frac{2\sqrt{\frac{70}{421}}}{3}$	0	$-\frac{4\sqrt{\frac{35}{421}}}{3}$	0	$-\frac{4\sqrt{\frac{35}{421}}}{3}$
B_8^3	$\frac{20\sqrt{\frac{7}{3937}}}{3}$	$\frac{20\sqrt{\frac{7}{3937}}}{3}$	$\frac{40\sqrt{\frac{7}{3937}}}{3}$	$\frac{10\sqrt{\frac{14}{3937}}}{3}$	$20\sqrt{\frac{7}{3937}}$	$\frac{10\sqrt{\frac{7}{3937}}}{3}$	$-\frac{50\sqrt{\frac{14}{3937}}}{3}$	0	$-\frac{20\sqrt{\frac{7}{3937}}}{3}$	0	$-\frac{20\sqrt{\frac{7}{3937}}}{3}$
$B_8^{\bar{6}_1}$	$-20\sqrt{\frac{7}{2869}}$	$20\sqrt{\frac{7}{2869}}$	0	$2\sqrt{\frac{14}{2869}}$	$-20\sqrt{\frac{7}{2869}}$	$18\sqrt{\frac{7}{2869}}$	$-2\sqrt{\frac{14}{2869}}$	$-40\sqrt{\frac{14}{2869}}$	$60\sqrt{\frac{7}{2869}}$	$-40\sqrt{\frac{7}{2869}}$	$20\sqrt{\frac{7}{2869}}$
$B_8^{15_1}$	$-460\sqrt{\frac{7}{1330969}}$	$-20\sqrt{\frac{133}{70051}}$	$-840\sqrt{\frac{7}{1330969}}$	$-78\sqrt{\frac{14}{1330969}}$	$460\sqrt{\frac{7}{1330969}}$	$626\sqrt{\frac{7}{1330969}}$	$246\sqrt{\frac{14}{1330969}}$	$-80\sqrt{\frac{14}{1330969}}$	$92\sqrt{\frac{7}{1330969}}$	$80\sqrt{\frac{7}{1330969}}$	$4\sqrt{\frac{133}{70051}}$
$B_8^{15_2}$	$20\sqrt{\frac{6}{871}}$	$-10\sqrt{\frac{6}{871}}$	$10\sqrt{\frac{6}{871}}$	$28\sqrt{\frac{3}{871}}$	$-20\sqrt{\frac{6}{871}}$	$-6\sqrt{\frac{6}{871}}$	$-32\sqrt{\frac{3}{871}}$	$60\sqrt{\frac{3}{871}}$	$-4\sqrt{\frac{6}{871}}$	$-30\sqrt{\frac{6}{871}}$	$2\sqrt{\frac{6}{871}}$
$B_{27}^{15_1}$	0	0	0	$-34\sqrt{\frac{14}{5281}}$	0	$-22\sqrt{\frac{7}{5281}}$	$-22\sqrt{\frac{14}{5281}}$	0	$-\frac{92\sqrt{\frac{7}{5281}}}{3}$	0	$-\frac{76\sqrt{\frac{7}{5281}}}{3}$
$B_{27}^{15_2}$	0	0	0	$8\sqrt{\frac{14}{453}}$	0	$-2\sqrt{\frac{7}{453}}$	$-2\sqrt{\frac{14}{453}}$	0	$4\sqrt{\frac{21}{151}}$	0	$-2\sqrt{\frac{21}{151}}$
$B_{27}^{24_1}$	0	0	0	$\sqrt{\frac{14}{3}}$	0	$-\sqrt{\frac{7}{3}}$	$-\sqrt{\frac{14}{3}}$	0	0	0	0

TABLE XVII: The inverse of the $SU(3)_F$ coefficient matrix given in Tabs. I and V of [23] which is used in order to map the fit example points of the topological approach onto the $SU(3)_F$ parameterization in Tabs. XV and XVI.

Decay amplitude	T	C	E	$P_{\rm break}$
$+\frac{1}{\sqrt{2}}\mathcal{A}(D^0\to\pi^+\pi^-)$	$-\frac{1}{\sqrt{2}}\times$ 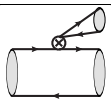	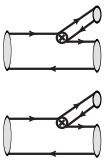	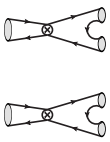	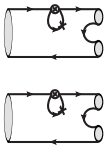
	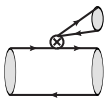			
	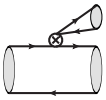	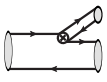		
	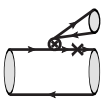	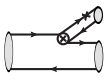		
	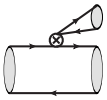	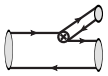	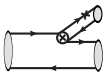	
	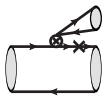			

Decay amplitude	T	$T_1^{(1)}$	$T_2^{(1)}$	E	$E_1^{(1)}$	$E_2^{(1)}$	P_{break}
$\mathcal{A}(D^0 \to K^+K^-)$	$1\times$ 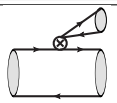	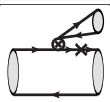	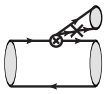				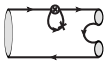
	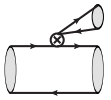						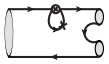
	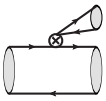	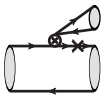					
	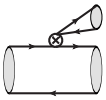		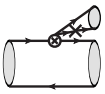				

Decay amplitude	T	$T_1^{(1)}$	$T_2^{(1)}$	$T_3^{(1)}$	A	$A_1^{(1)}$	$A_2^{(1)}$	$A_3^{(1)}$	C	$C_1^{(1)}$	$C_2^{(1)}$	$C_3^{(1)}$	P_{break}
$-\mathcal{A}(D^+ \to \bar{K}^0 K^+)$	$-1\times$	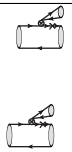			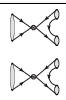								

Decay amplitude	T	$T_1^{(1)}$	$T_2^{(1)}$	A	$A_1^{(1)}$	$A_2^{(1)}$	$A_3^{(1)}$	C	$C_1^{(1)}$	$C_2^{(1)}$	$C_3^{(1)}$	P_{break}
$\sqrt{2}\mathcal{A}(D^+ \to \pi^0\pi^+)$	$-1\times$ 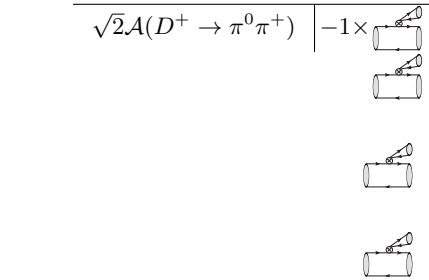											

[1] G. Altarelli, N. Cabibbo, and L. Maiani, Nucl.Phys. **B88**, 285 (1975).
[2] R. Kingsley, S. Treiman, F. Wilczek, and A. Zee, Phys.Rev. **D11**, 1919 (1975).
[3] M. Einhorn and C. Quigg, Phys.Rev. **D12**, 2015 (1975).
[4] M. Voloshin, V. Zakharov, and L. Okun, JETP Lett. **21**, 183 (1975).
[5] N. Cabibbo and L. Maiani, Phys.Lett. **B73**, 418 (1978).
[6] C. Quigg, Z.Phys. **C4**, 55 (1980).
[7] L.-L. Wang and F. Wilczek, Phys.Rev.Lett. **43**, 816 (1979).
[8] G. Eilam and J. Leveille, Phys.Rev.Lett. **44**, 1648 (1980).
[9] L.-L. Chau Wang, BNL-27615, C80-01-05-20, Talk at the Conference on Theoretical Particle Physics, 5-14 January 1980, Guangzhou (Canton), China, p. 1218.
[10] D. Zeppenfeld, Z.Phys. **C8**, 77 (1981).
[11] L.-L. Chau, Phys.Rept. **95**, 1 (1983).
[12] M. Golden and B. Grinstein, Phys.Lett. **B222**, 501 (1989).
[13] M. Gronau, O. F. Hernandez, D. London, and J. L. Rosner, Phys.Rev. **D50**, 4529 (1994), hep-ph/9404283.
[14] B. Bhattacharya and J. L. Rosner, Phys.Rev. **D81**, 014026 (2010), 0911.2812.
[15] L. Chau and H. Cheng, Phys.Rev.Lett. **56**, 1655 (1986).
[16] L.-L. Chau and H.-Y. Cheng, Phys.Rev. **D36**, 137 (1987).
[17] L.-L. Chau and H.-Y. Cheng, Phys.Lett. **B280**, 281 (1992).
[18] M. J. Savage, Phys.Lett. **B257**, 414 (1991).
[19] M. Gronau, O. F. Hernandez, D. London, and J. L. Rosner, Phys.Rev. **D52**, 6356 (1995), hep-ph/9504326.
[20] B. Grinstein and R. F. Lebed, Phys.Rev. **D53**, 6344 (1996), hep-ph/9602218.
[21] H.-Y. Cheng and C.-W. Chiang, Phys.Rev. **D81**, 074021 (2010), 1001.0987.
[22] D. Pirtskhalava and P. Uttayarat, Phys.Lett. **B712**, 81 (2012), 1112.5451.
[23] G. Hiller, M. Jung, and S. Schacht, Phys.Rev. **D87**, 014024 (2013), 1211.3734.
[24] E. Franco, S. Mishima, and L. Silvestrini, JHEP **1205**, 140 (2012), 1203.3131.
[25] H.-Y. Cheng and C.-W. Chiang, Phys.Rev. **D85**, 034036 (2012), 1201.0785.
[26] T. Feldmann, S. Nandi, and A. Soni, JHEP **1206**, 007 (2012), 1202.3795.
[27] J. Brod, Y. Grossman, A. L. Kagan, and J. Zupan, JHEP **1210**, 161 (2012), 1203.6659.
[28] B. Bhattacharya, M. Gronau, and J. L. Rosner, Phys.Rev. **D85**, 054014 (2012), 1201.2351.
[29] Y. Grossman and D. J. Robinson, JHEP **1304**, 067 (2013), 1211.3361.
[30] D. Fakirov and B. Stech, Nucl.Phys. **B133**, 315 (1978).
[31] W. Bernreuther, O. Nachtmann, and B. Stech, Z.Phys. **C4**, 257 (1980).
[32] H.-n. Li, C.-D. Lu, and F.-S. Yu, Phys.Rev. **D86**, 036012 (2012), 1203.3120.
[33] A. Buras, J. Gerard, and R. Ruckl, Nucl.Phys. **B268**, 16 (1986).
[34] M. Wiebusch, Comput.Phys.Commun. **184**, 2438 (2013), 1207.1446.
[35] D. Kraft, *A software package for sequential quadratic programming* (1988), Tech. Rep. DFVLR-FB 88-28, DLR German Aerospace Center Institute for Flight Mechanics, Köln, Germany.
[36] E. Jones, T. Oliphant, P. Peterson, et al., *SciPy: Open source scientific tools for Python* (2001–), URL `http://www.scipy.org/`.
[37] A. J. Buras and L. Silvestrini, Nucl.Phys. **B569**, 3 (2000), hep-ph/9812392.
[38] S. Glashow, J. Iliopoulos, and L. Maiani, Phys.Rev. **D2**, 1285 (1970).
[39] G. 't Hooft, Nucl.Phys. **B72**, 461 (1974).
[40] C. Sorensen, Phys.Rev. **D23**, 2618 (1981).
[41] F. Buccella, M. Lusignoli, G. Miele, A. Pugliese, and P. Santorelli, Phys.Rev. **D51**, 3478 (1995), hep-ph/9411286.
[42] F. Buccella, M. Lusignoli, A. Pugliese, and P. Santorelli, Phys.Rev. **D88**, 074011 (2013), 1305.7343.
[43] M. Neubert, Phys.Lett. **B424**, 152 (1998), hep-ph/9712224.
[44] C. Smith, Eur.Phys.J. **C10**, 639 (1999), hep-ph/9808376.
[45] B. Bhattacharya, M. Gronau, and J. L. Rosner (2012), 1207.6390.
[46] J. Beringer et al. (Particle Data Group), Phys.Rev. **D86**, 010001 (2012), and 2013 partial update for the 2014 edition.
[47] A. Zupanc et al. (Belle Collaboration), JHEP **1309**, 139 (2013), 1307.6240.
[48] P. Onyisi et al. (CLEO Collaboration), Phys.Rev. **D88**, 032009 (2013), 1306.5363.
[49] D. Epifanov et al. (Belle Collaboration), Phys.Lett. **B654**, 65 (2007), 0706.2231.
[50] J. H. Kuhn and E. Mirkes, Z.Phys. **C56**, 661 (1992).
[51] S. Wilks, Annals Math.Statist. **9**, 60 (1938).
[52] I. I. Bigi and H. Yamamoto, Phys.Lett. **B349**, 363 (1995), hep-ph/9502238.
[53] J. L. Rosner, Phys.Rev. **D74**, 057502 (2006), hep-ph/0607346.
[54] D.-N. Gao, Phys.Lett. **B645**, 59 (2007), hep-ph/0610389.
[55] D.-N. Gao, Phys.Rev. **D91**, 014019 (2015), 1411.0768.
[56] M. Beneke, G. Buchalla, M. Neubert, and C. T. Sachrajda, Phys.Rev.Lett. **83**, 1914 (1999), hep-ph/9905312.
[57] M. Beneke, G. Buchalla, M. Neubert, and C. T. Sachrajda, Nucl.Phys. **B606**, 245 (2001), hep-ph/0104110.
[58] M. T. Hansen and S. R. Sharpe, Phys.Rev. **D86**, 016007 (2012), 1204.0826.
[59] D. Binosi and L. Theussl, Comput.Phys.Commun. **161**, 76 (2004), hep-ph/0309015.
[60] J. Vermaseren, Comput.Phys.Commun. **83**, 45 (1994).
[61] Y. Amhis et al. (Heavy Flavor Averaging Group) (2012), 1207.1158, and online update 30 June 2014.
[62] G. Bonvicini et al. (CLEO Collaboration), Phys.Rev. **D89**, 072002 (2014), 1312.6775.
[63] A. Zupanc for the Belle Collaboration, Talk at the 6th International Workshop on Charm Physics, 31 August-4 September 2013, Manchester, UK.
[64] C. Liu (2012), 1207.1171.
[65] D. Besson et al. (CLEO Collaboration), Phys.Rev. **D80**, 032005 (2009), 0906.2983.
[66] L. Widhalm et al. (Belle Collaboration), Phys.Rev.Lett. **97**, 061804 (2006), hep-ex/0604049.
[67] B. Aubert et al. (BaBar Collaboration), Phys.Rev. **D76**,

052005 (2007), 0704.0020.
[68] J. Koponen, C. Davies, and G. Donald (HPQCD Collaboration) (2012), 1208.6242.
[69] J. Koponen, C. Davies, G. Donald, E. Follana, G. Lepage, et al. (2013), 1305.1462.
[70] A. Hocker, H. Lacker, S. Laplace, and F. Le Diberder, Eur.Phys.J. **C21**, 225 (2001), hep-ph/0104062.
[71] G. Hiller, M. Jung and S. Schacht, in preparation, DO-TH 13/25, QFET-2013/12, TTP13-037.
[72] V. D. Barger and S. Pakvasa, Phys.Rev.Lett. **43**, 812 (1979).
[73] A. Ali, G. Kramer, and C.-D. Lu, Phys.Rev. **D58**, 094009 (1998), hep-ph/9804363.